

**APPLICATIONS OF RIGID-PLASTIC FINITE ELEMENT ANALYSIS  
USING EULERIAN MESHING SCHEME TO SIMULATE FORGING  
AND SHEET METAL CLINCHING PROCESSES**

By

**CHEONG WEN CHIET**

A dissertation submitted to the Department of Mechanical and Material  
Engineering,  
Lee Kong Chian Faculty of Engineering Science,  
Universiti Tunku Abdul Rahman,  
in partial fulfilment of the requirements for the degree of Master of  
Engineering Science  
January 2015

## **ABSTRACT**

# **APPLICATIONS OF RIGID-PLASTIC FINITE ELEMENT ANALYSIS USING EULERIAN MESHING SCHEME TO SIMULATE FORGING AND SHEET METAL CLINCHING PROCESSES**

**Cheong Wen Chiet**

During forging process, large deformation of workpiece normally lead to heavily distorted elements in finite element analysis. Consequently, numerical calculation becomes not stable and affects the convergence of non-linear solution. Rigid-plastic finite element method by using the Eulerian meshing scheme was applied to deal with large deformation problem and to treat remeshing issue. With Eulerian scheme, elements were initially generated into an analytical zone with markers implanted to form the workpiece. Markers will flow between elements during deformation step and show the material flow of workpiece. Besides, the study of sensitivity for mesh size and time step was carried out in Eulerian scheme. Four types of cold forging and sheet metal clinching were conducted to investigate the effectiveness of Eulerian scheme by comparing the results on extruded shape of the final product, the punch load versus punch stroke graph and computational time obtained from simulation and experiment. The results were in good agreement.

## **ACKNOWLEDGEMENT**

First and foremost, I would like to express my sincere and deepest appreciation to my supervisor, Dr. Wang Chan Chin, for his invaluable guidance and advice on my work. I was able to gain a lot of skills, knowledge and experiences from him. In addition, I wish to sincerely express gratitude to my co-supervisor, Dr. Lim Ying Pio, who had provided me continuous guidance, directions and advice when I was conducting my works.

Furthermore, I acknowledge the faculty and the staff of the Department of Mechanical Engineering in Universiti Tunku Abdul Rahman and Tunku Abdul Rahman College, who have provided me with the most cooperative assistance to my research work.

Last but not least, a big appreciation is dedicated to my beloved family and friends who have given me encouragement and motivation throughout my entire study.

## **APPROVAL SHEET**

This dissertation entitled "**APPLICATIONS OF RIGID-PLASTIC FINITE ELEMENT ANALYSIS USING EULERIAN MESHING SCHEME TO SIMULATE FORGING AND SHEET METAL CLINCHING PROCESSES**" was prepared by CHEONG WEN CHIET and submitted as partial fulfilment of the requirements for the degree of Master of Engineering Science at Universiti Tunku Abdul Rahman.

Approved by:

(Dr. WANG CHAN CHIN)

### **Supervisor**

Department of Mechanical and Material Engineering  
Faculty of Engineering Science  
Universiti Tunku Abdul Rahman

Date: .....

---

(Dr. LIM YING PIO)

### Co-Supervisor

Co-Supervisor  
Department of Mechanical and Material Engineering  
Faculty of Engineering Science  
Universiti Tunku Abdul Rahman

Date:

**FACULTY OF ENGINEERING AND SCIENCE**

**UNIVERSITI TUNKU ABDUL RAHMAN**

Date: 19 January 2015

**SUBMISSION OF THESIS**

It is hereby certified that **CHEONG WEN CHIET** (ID No: **09UEM09194**) has completed this dissertation entitled "**APPLICATIONS OF RIGID-PLASTIC FINITE ELEMENT ANALYSIS USING EULERIAN MESHING SCHEME TO SIMULATE FORGING AND SHEET METAL CLINCHING PROCESSES**" under the supervision of Dr. WANG CHAN CHIN (Supervisor) from the Department of Mechanical and Material Engineering, Faculty of Engineering and Science, and Dr. LIM YING PIO (Co-Supervisor) from the Department of Mechanical and Material Engineering, Faculty of Engineering and Science.

I understand that the University will upload softcopy of my thesis in pdf format into UTAR Institutional Repository, which may be made accessible to UTAR community and public.

Yours truly,

---

(CHEONG WEN CHIET)

## **DECLARATION**

I hereby declare that the dissertation is based on my original work except for quotations and citations which have been duly acknowledged. I also declare that it has not been previously or concurrently submitted for any other degree at UTAR or other institutions.

---

(CHEONG WEN CHIET)

Date \_\_\_\_\_

## TABLE OF CONTENTS

	<b>Page</b>
ABSTRACT	ii
ACKNOWLEDGEMENT	iii
APPROVAL SHEET	iv
SUBMISSION OF THESIS	v
DECLARATION	vi
TABLE OF CONTENTS	vii
LIST OF TABLES	x
LIST OF FIGURES	xiii
LIST OF ABBREVIATIONS	xix
LIST OF NOTATIONS	xx

## **CHAPTER**

1.0 INTRODUCTION	1
1.1 Research Background	1
1.2 Research Objectives	2
1.3 Thesis Overview	3
2.0 LITERATURE REVIEW	4
2.1 Introduction	4
2.2 Applications of FEM on Metal Forming	5
2.3 Meshing Schemes in FEM	7
2.3.1 Lagrangian and Eulerian Meshing	7

2.3.2	Arbitrary Lagrangian-Eulerian (ALE) FEM	8
2.3.3	Meshless Method	9
<b>3.0</b>	<b>FINITE ELEMENT FORMULATION</b>	<b>11</b>
3.1	Rigid-Plastic Finite Element Method	11
3.2	Meshing Method	13
3.2.1	Eulerian Scheme	15
3.2.1.1	Defining an Analytical Zone	16
3.2.1.2	Searching the Tool Boundaries	17
3.2.1.3	Before Solving the Matrix	19
3.2.1.4	Constructing and Solving the Matrix	20
3.2.1.5	After Solving the Matrix	21
<b>4.0</b>	<b>METHODOLOGY</b>	<b>22</b>
4.1	Introduction	22
4.2	Material Property	23
4.3	Extrusions and Sheet Metal Clinching	27
4.3.1	Extrusions	28
4.3.2	Sheet Metal Clinching	30
4.4	FEM Simulation	31
<b>5.0</b>	<b>VALIDATION BETWEEN SIMULATION AND EXPERIMENTAL RESULT</b>	<b>33</b>
5.1	Introduction	33
5.2	Backward Extrusion	34

5.2.1	Sensitivity of Mesh Size	36
5.2.1.1	Condition 1	38
5.2.1.2	Condition 2	40
5.2.1.3	Condition 3	42
5.2.2	Sensitivity of Time Step	44
5.2.2.1	Condition 1	44
5.2.2.2	Condition 2	46
5.2.2.3	Condition 3	48
5.2.3	Conclusion	51
5.3	Forward-Backward Extrusion	55
5.4	Double Cup Extrusion	57
5.5	Axi-Symmetric Ring Cup Extrusion	59
5.6	Sheet Metal Clinching	61
6.0	CONCLUSIONS AND FUTURE WORK	63
6.1	Conclusions	63
6.2	Contributions	64
6.3	Future Work	65
	REFERENCES	66
	APPENDICES	69

## LIST OF TABLES

<b>Table</b>		<b>Page</b>
2.1	Comparison of advantages and disadvantages for each meshing method	10
4.1	Material properties and working conditions for the simulation	25
4.2	Parameters for mesh size and time step	32
5.1	Conditions used to study the sensitivity of mesh size in backward extrusion	36
5.2	Comparison of punch loads between experiment and calculations for different mesh size in backward extrusion at time step = 0.005s/step	39
5.3	Comparison of punch loads between experiment and calculations for different mesh sizes in backward extrusion at time step = 0.05s/step	41
5.4	Comparison of punch loads between experiment and calculations for different mesh sizes in backward extrusion at time step = 0.5s/step	43

5.5	Conditions used to study the effect of mesh size in backward extrusion	44
5.6	Comparison of punch loads between experiment and calculations for different time steps in backward extrusion with mesh size = 0.3mm	46
5.7	Comparison of punch loads between experiment and calculations for different time steps in backward extrusion with mesh size = 0.5mm	48
5.8	Comparison of punch loads between experiment and calculations for different time steps in backward extrusion with mesh size = 0.7mm	50
5.9	Computational time	51
5.10	Percentage error for all simulation parameters	51
5.11	Comparison of punch loads between experiment and calculation in forward-backward extrusion (mesh size $M = 0.5\text{mm}$ and time step $T = 0.05\text{s/step}$ )	56

5.12	Comparison of punch loads between experiment and calculation in double cup extrusion  (mesh size $M = 0.5\text{mm}$ and time step $T = 0.05\text{s/step}$ )	58
5.13	Comparison of punch loads between experiment and calculation in axi-symmetric ring cup extrusion  (mesh size $M = 0.5\text{mm}$ and time step $T = 0.05\text{s/step}$ )	60
5.14	Comparison of punch loads between experiment and calculation in sheet metal clinching  (mesh size $M = 0.5\text{mm}$ and time step $T = 0.05\text{s/step}$ )	62

## LIST OF FIGURES

<b>Figure</b>		<b>Page</b>
3.1	Isoparametric quadrilateral element for Lagrange's mesh	14
3.2	Simulation of backward extrusion using Lagrange's elements (Courtesy from RIPLS-FORGE)	14
3.3	Steps for Eulerian mesh in simulating a metal forming	15
3.4	Defining analytical zone in backward extrusion using Eulerian mesh	16
3.5	Searching for boundary lines in Eulerian mesh	18
4.1	Flow of research	22
4.2	Compression test	23
4.3	Tensile test for steel metal sheet	24
4.4	Tooling setup for extrusion processes	27
4.5	Backward extrusion	28

4.6	Forward-backward extrusion	29
4.7	Double cup extrusion	29
4.8	Axi-symmetric ring cup extrusion	30
4.9	Sheet metal clinching	30
4.10	Stages in FEM simulation	31
5.1	Mesh size	34
5.2	Different mesh size $M$ in backward extrusion	35
5.3	Polynomial approximation of punch load curve (time step $T = 0.005\text{s}/\text{step}$ and mesh size $M = 0.5\text{mm}$ )	37
5.4	Extruded shapes for different mesh sizes in backward extrusion at time step = $0.005\text{s}/\text{step}$	38
5.5	Comparison of punch load curves between experimental and calculations for different mesh sizes in backward extrusion at time step = $0.005\text{s}/\text{step}$	39

5.6	Extruded shapes for different mesh sizes in backward extrusion at time step = 0.05s/step	40
5.7	Comparison of punch load curves between experimental and calculations for different mesh sizes in backward extrusion at time step = 0.05s/step	41
5.8	Extruded shapes for different mesh sizes in backward extrusion at time step = 0.5s/step	42
5.9	Comparison of punch loads between experimental and calculations for different mesh sizes in backward extrusion at time step = 0.5s/step	43
5.10	Extruded shapes for different time steps in backward extrusion at mesh size = 0.3mm	45
5.11	Comparison of punch load curves between experiment and calculations for different time steps in backward extrusion with mesh size = 0.3mm	45
5.12	Extruded shapes for different time steps in backward extrusion at mesh size = 0.5mm	47

5.13	Comparison of punch load curves between experiment and calculations for different time steps in backward extrusion with mesh size = 0.5mm	47
5.14	Extruded shapes for different time steps in backward extrusion with mesh size = 0.7mm	49
5.15	Comparison of punch load curves between experiment and calculations for different time steps in backward extrusion with mesh size = 0.7mm	49
5.16	Boundary line for different mesh size	52
5.17	Element with no marker	53
5.18	Comparison of extruded shape between experiment and calculation for backward extrusion (mesh size $M = 0.5\text{mm}$ , time step $T = 0.05\text{s}/\text{step}$ and experimental punch rate = 2mm/min)	54
5.19	Comparison for extruded shapes between experiment and calculation in forward-backward extrusion (mesh size $M = 0.5\text{mm}$ , time step $T = 0.05\text{s}/\text{step}$ and experimental punch rate = 2mm/min)	55

5.20	Comparison of punch load curves between experiment and calculation in forward-backward extrusion (mesh size $M = 0.5\text{mm}$ and time step $T = 0.05\text{s}/\text{step}$ )	56
5.21	Comparison for extruded shapes between experiment and calculation in double cup extrusion (mesh size $M = 0.5\text{mm}$ , time step $T = 0.05\text{s}/\text{step}$ and experimental punch rate = 2mm/min)	57
5.22	Comparison of punch load curves between experiment and calculation in double cup extrusion (mesh size $M = 0.5\text{mm}$ and time step $T = 0.05\text{s}/\text{step}$ )	58
5.23	Comparison for extruded shapes between experiment and calculation in axi-symmetric ring cup extrusion (mesh size $M = 0.5\text{mm}$ , time step $T = 0.05\text{s}/\text{step}$ and experimental punch rate = 2mm/min)	59
5.24	Comparison of punch load curves between experiment and calculation in axi-symmetric ring cup extrusion (mesh size $M = 0.5\text{mm}$ and time step $T = 0.05\text{s}/\text{step}$ )	60
5.25	Comparison for extruded shapes between experiment and calculation in sheet metal clinching (mesh size $M = 0.5\text{mm}$ and time step $T = 0.05\text{s}/\text{step}$ )	61

5.26 Comparison of punch load curves between experiment  
and calculation in sheet metal clinching  
(mesh size  $M = 0.5\text{mm}$  and time step  $T = 0.05\text{s/step}$ )

## **LIST OF ABBREVIATIONS**

ALPID	Analysis of Large Plastic Incremental Deformation
ALE	Arbitrary Lagrangian-Eulerian
FEM	Finite Element Method
FEA	Finite Element Analysis
NEM	Natural Element Method
SNAW	Structural Nonlinear Analysis Workspace
SCNI	Stabilized Conforming Nodal Integration

## LIST OF NOTATIONS

$\sigma_{ij}'$	Deviatoric stress tensor
$\bar{\sigma}$	Flow stress
$\sigma_m$	Hydrostatic stress
$F$	Magnitude of flow stress
$M$	Mesh size
$g$	Small positive value (0.01-0.0001)
$\bar{\varepsilon}$	Strain
$\dot{\varepsilon}$	Strain rate
$\sigma$	Stress
$T$	Time step
$\dot{\varepsilon}_v$	Volumetric strain rate
$n$	Work hardening exponent

# **CHAPTER 1**

## **INTRODUCTION**

### **1.1 Research Background**

In metal forming such as forging and deep drawing, the contact surfaces between tools, workpiece and dies will undergo severe working condition of large deformation and highly localised surface pressure. Therefore, the final dimension of product and the life span of tools are the main concerns in industry. However, most of the tooling design and process design for metal forming are still heavily relied on engineer experiences or conventional experimental methods by trial and error. Therefore, Finite Element Method (FEM) has become a popular tool to analyse and optimise metal forming operations.

Many commercial FEM codes like Deform, Forge2, Forge3 and Indeed are widely utilised in industry to design and optimise forming processes. However, under large deformation such as forging, elements in Finite Element Analysis (FEA) will be heavily distorted and lead to instability of numerical calculation. Although remeshing is a technique to replace distorted elements but the tendency of volume loss after each remeshing procedure will affect the result. In addition, the computation time will be increased significantly since the remeshing procedure is required almost on every deformation step.

Thus, Eulerian meshing method based on rigid-plastic finite element was developed and applied in this study to treat the remeshing issue. Investigations were carried out to study the behaviour of Eulerian mesh and the sensitivities for mesh size and time step in backward extrusion. The appropriate parameters for mesh size and time steps were applied to others metal forming processes such as forward-backward extrusion, double cup extrusion, axi-symmetric ring cup extrusion and sheet metal clinching. Effectiveness of the application of Eulerian mesh was examined by comparing the results from FEM simulation and experiment.

## **1.2      Research Objectives**

The objectives of this study were:-

1. To study the behaviours of Eulerian mesh and sensitivities for mesh size and time step in FEM simulation of metal forming such as forging and sheet metal clinching.
2. To study the effectiveness of Eulerian mesh in backward extrusion, forward-backward extrusion, double cup extrusion, axi-symmetric ring cup extrusion and sheet metal clinching.

### **1.3 Thesis Overview**

This thesis consists of six chapters. Chapter 1 presents an introduction, the objectives and the layout of the thesis. Chapter 2 covers literature review and the topics mainly discuss the applications of FEM on metal forming and different meshing schemes studied by researchers. Chapter 3 presents the formulation of rigid-plastic finite element method. The description of Eulerian meshing scheme is highlighted. In Chapter 4, methodology to conduct experiment and simulation are covered with the steps on how to obtain material properties and conduct forging and sheet metal clinching processes on a universal testing machine. Besides, dimension of tools, dies and billet are listed in this chapter. Chapter 5 discusses the sensitivities for mesh size and time step of Eulerian mesh and the validation between simulation and experimental results for backward extrusion, forward-backward extrusion, double cup extrusion, axi-symmetric ring cup extrusion and sheet metal clinching. Chapter 6 describes the conclusions and the contributions of this study and the plans for future work.

## **CHAPTER 2**

### **LITERATURE REVIEW**

#### **2.1 Introduction**

In metal forming, a workpiece is usually formed into a complex geometry product through several operations. Production cost, time, accuracy and performance of the final product are the crucial factors to be considered in industry, but the planning of metal forming process and die design are normally relied on empirical knowledge and experience or even undergo trial and error methods. Therefore, Finite Element Method (FEM) has become a reliable tool to obtain optimum design for tooling, dies and forming processes. It can be used to predict metal flow, final dimension of the part, prevent flow induced defects and predict the temperature (Altan et al., 2003).

Numerous studies had been carried out to implement the applications of FEM in analyzing metal forming processes.

## 2.2 Applications of FEM on Metal Forming

The upper-bound method has been adapted for many years in metal forming simulation. This method involves admissible velocity field to analyze metal flow. However, it is extremely difficult if the geometry and metal flow of the workpiece is complicated. Therefore, it is only applicable to simple problems.

Among various methods, rigid-plastic FEM appeared to be a reliable method in analyzing plastic flow problem. With the concepts of elements and trial function, rigid-plastic FEM is free of geometrical restriction and it is possible to analyze wide range of boundary conditions. It is because the construction of variational functional and derivatives are at elemental level. Oh et al. (1982) discussed the rigid-plastic FEM and upper-bound method and further developed a computer program called Analysis of Large Plastic Incremental Deformation (ALPID) to compare the simulation and experimental results of upsetting, ring compression and spike forging. The proposed method was flexible and the results were accurate.

By using the Lévy-von Mises criterion, the stress in rigid-plastic FEM is determined without the reference of the previous step. Besides, elastic deformation is neglected in rigid-plastic FEM. Thus, the computational time is shorter compared to elastic-plastic FEA. Work hardening and shape change are incorporated in the formulation presented by Osaka et al. (1982). This formulation provides more accurate results in treating non-steady problems and

unstable mode of deformation when compared to the extended method for infinitesimal deformation. Mori et al. (1996) combined the effect of elastic deformation in a rigid-plastic FEM to simulate a plane-strain bending of a plate. The authors equilibrated the nodal force between rigid-plastic, elastic and elastic-plastic elements at the end of each deformation step under implicit scheme. The value of equivalent stress in the rigid region was reduced with the decrease in equivalent strain-rate to approximate elastic deformation during loading, residual stress and spring back after unloading.

Many elasto-plastic finite element codes employed using the implicit time integration scheme because larger computational time could be taken for establishing the tangent stiffness matrices and solved in an iterative manner for each load step. However, the calculations in implicit scheme often stopped due to lack of convergence (Makinouchi, 1991). Besides, dynamic equations for explicit scheme were solved with small time steps. Explicit scheme was stable when dealing with large and especially 3D problems (Behzad et al., 1994).

## **2.3 Meshing Schemes in FEM**

### **2.3.1 Lagrangian and Eulerian Meshing**

Lagrangian and Eulerian formulation are widely used in finite element simulation to deal with metal forming. The finite element mesh for Lagrangian approach is attached on the workpiece and followed its deformation. For Eulerian formulation, the mesh is fixed in space while the material flowed between the elements. Lagrangian scheme is suitable for unconstrained flow. Although it is easier to implement and fast in converging but severe distortion of elements and mesh entanglement are the main difficulties when deal with large deformation and non linear boundary condition problems.

Eulerian formulation is an approach for fluid mechanics problems and it is suitable for large material flow and minimal change in boundary shapes problems. No remeshing is required since the mesh is fixed in space.

Under severe metal forming condition between workpiece, dies and tools, issue of highly distorted elements for simulation normally inevitable and caused instability in FEM calculation. Remeshing is a technique to overcome the distorted element but it is almost required on every step of the simulation. No doubt, the computational time required will be increased and the accuracy will be affected tremendously. Mori et al. (1983) introduced an idea of defining the elements to an unchanged spatial grid rather than on a workpiece to treat the remeshing issue. Monitoring points which carried information of

the equivalent strain were embedded in the deforming material while the elements remain unchanged. Simulation of backward extrusion of cans was carried out and showed promising results.

### 2.3.2 Arbitrary Lagrangian-Eulerian (ALE) FEM

Arbitrary Lagrangian-Eulerian (ALE) FEM is the combination feature of both Lagrangian and Eulerian approaches. In ALE, each degree of freedom of the system may be assigned an arbitrary motion independent of the material deformation. The ALE may to avoid remeshing. However, the unique issue for ALE is the mesh velocities for all degree of freedom in each incremental has to be assigned by analyst. Therefore, Gadala et al. (2002) proposed the designing mesh motion scheme in ALE analysis.

In classical Lagrangian formulation, a very large number of useless meshes have to be considered. Boman et al. (2006) raised up an example regarding the issue mentioned above where the tools for a roll forming had to be finely discretized although the tools do not required a refined mesh in the stationary state. Consequently, the computational time was large. The authors introduced ALE formulation to divide the time step into 2 phases which were Lagragian and ALE. ALE is the rezoning phase where the nodes were moved and the values stored at Gauss points were updated after the Eulerian phase.

Willaims et al. (2010) presented a mixed Eulerian-Lagrangian approach to deal remeshing problem on extrusion. The workpiece was modelled with

Eulerian finite volume method as a non-Newtonian ‘plastic’ fluid on a fixed mesh and the die was using Lagrangian technique since the deformation was minimal on die. Besides, this method avoided the need for explicit contact analysis which helps to prevent remeshing.

### 2.3.3 Meshless Method

Meshless methods are based on the employ of scattered data approximation techniques to construct the approximating space of the Galerkin method. Filice et al. (2009) adapted the natural element method (NEM) to simulate the extrusion of cross-shaped profile where this method constructed natural neighbour interpolation to employ trial and test function. After the comparison between FEM and NEM formulation, the authors concluded that meshless method showed promising results and no remeshing required but the main drawback was higher computational cost due to more time was needed to calculate the shape functions.

Edwin et al. (1999) introduced Structural Nonlinear Analysis Workspace (SNAW) meshless formulation based on the Reproducing Kernel Particle Method. The model refinement in this meshless computation can be accomplished by direct particle insertion and deletion without remeshing. SNAW was effectively dealt with irregular shaped structure

In order to improve the computational efficiency in Galerkin based meshfree method, an accelerated meshfree method was developed by Yoon and

Chen (2002). Strain smoothing stabilization procedure named stabilized conforming nodal integration (SCNI) method was presented to meet integration constrains, to eliminate spatial instability and to stabilize the nodal integration. Application of SCNI method on extrusion was presented and the results demonstrated significant improvement in computational efficiency.

Table 2.1: Comparison of advantages and disadvantages for each meshing method.

<b>Meshing Method</b>	<b>Advantages</b>	<b>Disadvantages</b>
Lagrangian	It is easier to implement and fast in converging	Remeshing issue when deal with large deformation and non liner boundary condition
Eulerian	No remeshing is required since the mesh is fixed in space	Higher usage of computer memory due to redundant of elements and markers
Arbitrary Lagrangian-Eulerian	It maintains the Eulerian form at locations with high deformation while reduced to Lagrangian form on free boundaries to avoid remeshing	Coupling issue between workpiece (Eulerian mesh) and die (Lagrangian mesh)
Meshless	No remeshing is required	Higher computational cost due to more time is needed to calculate the shape function

The computational cost for meshless method is higher compared to other and it had been estimated about four times higher in some research works (Alfaro et al., 2007). Besides, Williams et al. (2002) had encountered the coupling issue between Largrangian and Eulerian domain in mixed Eulerian-Lagraigian approach where the interaction between the two domains was only one way. Any changes of the Largragian domain were not reapplied into the Eulerian domain. Based on the pros and cons in Table 2.1, Eulerian meshing was chosen in this study to treat the remeshing issue.

## CHAPTER 3

### FINITE ELEMENT FORMULATION

#### 3.1 Rigid-Plastic Finite Element Method

Rigid-plastic and elasto-plastic analysis are the two main formulations in FEM to analyze metal forming processes. Rigid-plastic analysis is formulated based on the Lévy Von-Mises equations where the calculation for elastic deformation is not included. It is normally used to simulate bulk forming processes. The deformation behavior in bulk forming processes is assumed to be fully plastically deformed and undergo large deformation rather than elastic deformation. On the other hand, elasto-plastic analysis is based on Prandtl-Reuss equation and it is mainly used to deal with phenomenon associated with elasticity such as springback effect caused by elastic strain in sheet forming.

In order to approximate the plastic deformation and obey Von-Mises yield criterion as shown in Eq. (3.1), the mathematic models for the present finite element equations are based on the plasticity theory with slightly compressible rigid-plastic material (Osakada et al., 1982).

$$\bar{\sigma}^2 = \frac{3}{2} \sigma_{ij}' \sigma_{ij}' + g \sigma_m^2 \quad (3.1)$$

Where  $\sigma_{ij}'$  is the deviatoric stress tensor,  $g$  is the small positive value (0.01-0.0001),  $\sigma_m$  is the hydrostatic stress and  $\bar{\sigma}$  is the flow stress.

The flow stress can be expressed as a function of equivalent strain  $\bar{\varepsilon}$  and equivalent strain rate  $\dot{\bar{\varepsilon}}$  when dealing with word-hardening effect and visco-plastic behaviours. The stress  $\sigma$  and strain-rate  $\dot{\varepsilon}$  relationship for slightly compressible rigid-plastic material is derived from yield criterion of Eq. (3.1) by using associated rule;

$$\{\sigma\} = [D]\{\dot{\varepsilon}\} \quad (3.2)$$

$$\{\sigma\}^T = \{\sigma_x, \sigma_y, \sigma_z, \tau_{xy}, \tau_{yz}, \tau_{zx}\}$$

$$\{\dot{\varepsilon}\}^T = \{\dot{\varepsilon}_x, \dot{\varepsilon}_y, \dot{\varepsilon}_z, \dot{\gamma}_{xy}, \dot{\gamma}_{yz}, \dot{\gamma}_{zx}\}$$

$$[D] = \frac{\bar{\sigma}}{\dot{\bar{\varepsilon}}} \begin{bmatrix} a_1 & a_2 & a_2 & 0 & 0 & 0 \\ a_2 & a_1 & a_2 & 0 & 0 & 0 \\ a_2 & a_2 & a_1 & 0 & 0 & 0 \\ 0 & 0 & 0 & a_3 & 0 & 0 \\ 0 & 0 & 0 & 0 & a_3 & 0 \\ 0 & 0 & 0 & 0 & 0 & a_3 \end{bmatrix}$$

$$\text{Where } a_1 = \frac{1}{g} + \frac{4}{9}, a_2 = \frac{1}{g} + \frac{2}{9}, a_3 = \frac{1}{3}$$

The stress  $\sigma$  from the strain-rate  $\dot{\varepsilon}$  component in Eq. (3.2) is calculated directly due to the pressure sensitivity of the yield criterion. It is because the material undergoes volumetric change during plastic deformation. Less volumetric change will happen when the value of  $g$  decreases. A better approximation can be done with the incompressible condition.

The equivalent strain rate  $\dot{\bar{\varepsilon}}$  is defined as;

$$\dot{\bar{\varepsilon}}^2 = \frac{2}{3} \dot{\varepsilon}_{ij}' \dot{\varepsilon}_{ij}' + \frac{1}{g} \dot{\varepsilon}_v^2 \quad (3.3)$$

Where  $\dot{\varepsilon}_{ij}' = \dot{\varepsilon}_{ij} - \delta_{ij} \dot{\varepsilon}_v / 3$  and  $\dot{\varepsilon}_v$  is the volumetric strain rate.

The  $\frac{1}{g}$  in Eq. (3.3) is similar to the penalty function method in other rigid-plastic finite element approach. The compressibility in the plastic deformation becomes very small when the value of  $g$  is relatively small. This will be approximately satisfied the plasticity theory of incompressibility.

### 3.2 Meshing Method

Lagrange's element is the isoparametric quadrilateral elements with four nodal points as shown in Fig. 3.1. It is widely used in the commercial finite element simulator to deal with two-dimensional forging simulation. Since the mesh is attached in the workpiece, the shape of the elements will change drastically during deformation. Large shearing and compressive deformation especially around the corner between tools and workpiece will lead to heavily distorted elements as shown in Fig. 3.2. Remeshing is carried out to treat the instability of calculation and convergence of the solution caused by the heavily distorted elements. Consequently, the computational time is increased and the error of volume lost for each remeshing procedures will definitely reduce the overall accuracy of the result.

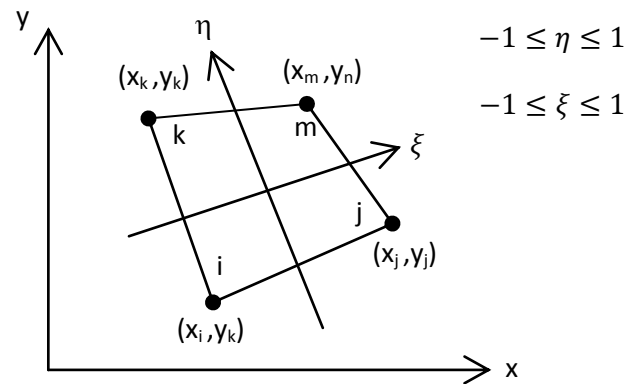


Figure 3.1: Isoparametric quadrilateral element for Lagrange's mesh.

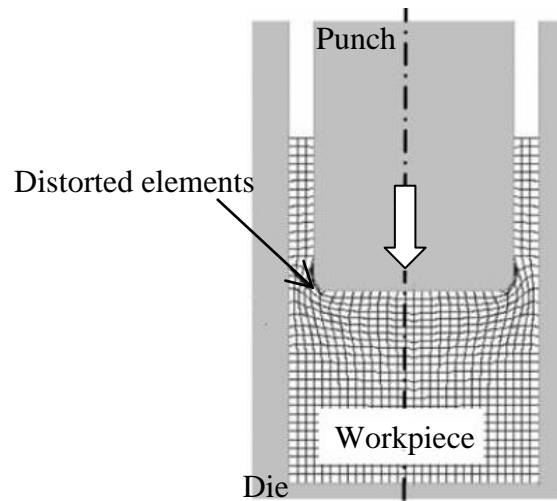


Figure 3.2: Simulation of backward extrusion using Lagrange's elements.

(Courtesy from RIPLS-FORGE)

### 3.2.1 Eulerian Scheme

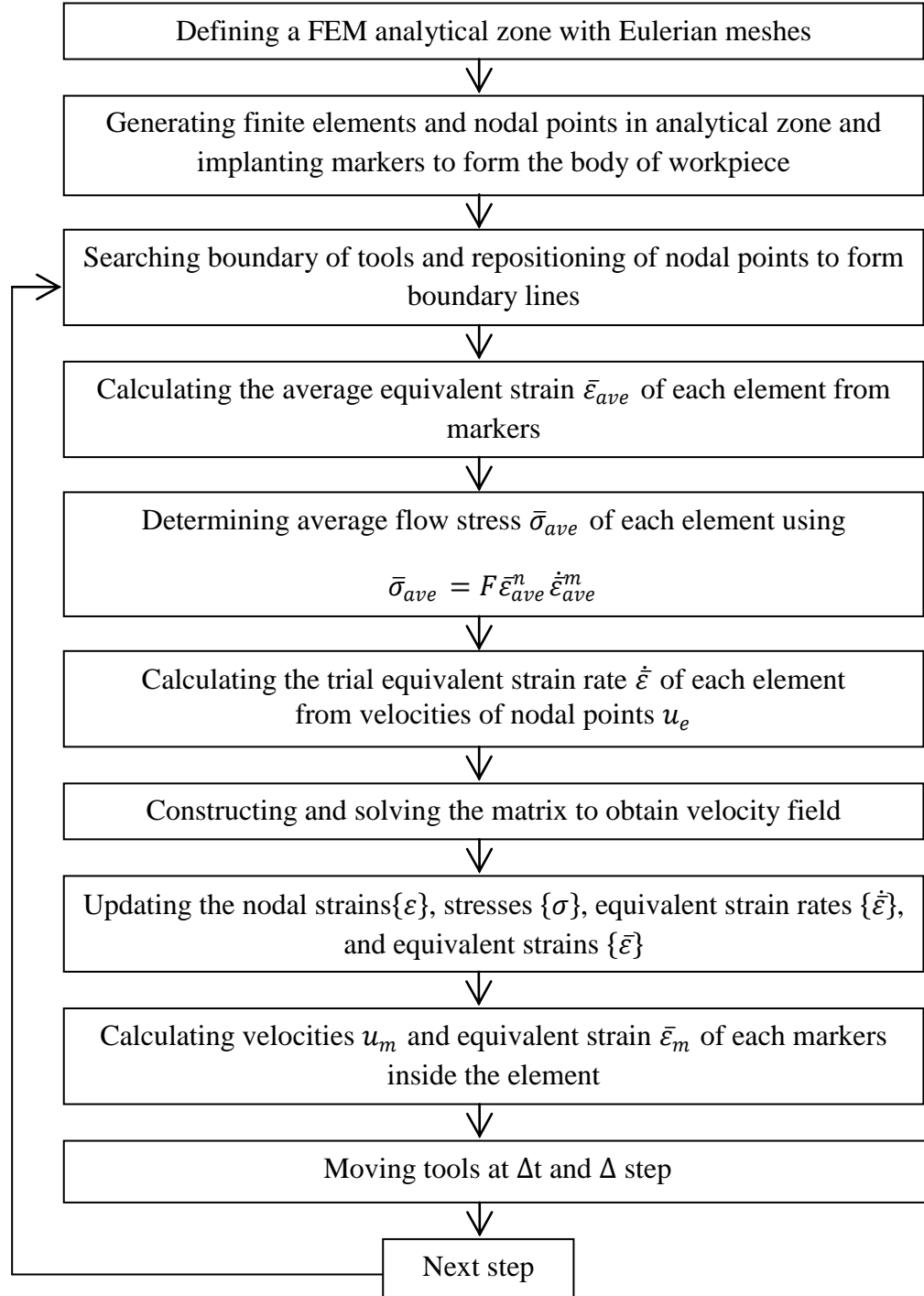


Figure 3.3: Steps for Eulerian mesh in simulating a metal forming.

In order to overcome the remeshing issue, Eulerian scheme based on infinitesimal deformation approach was applied in this study. The steps for

Eulerian scheme in simulating a metal forming process were shown in Fig 3.3.

The detail of the flow chart will be explained in the following sections.

### 3.2.1.1 Defining an Analytical Zone

Firstly, an analytical zone was defined to cover the workpiece and material deformation area for backward extrusion. Since the model chosen in the simulation was axi-symmetric, only half of the workpiece was meshed. Elements and nodal points were generated within the zone and the markers were implanted to represent the workpiece as shown in Fig. 3.4. The elements of Eulerian mesh will remain unchanged during deformation and only the markers were flowed between the elements.

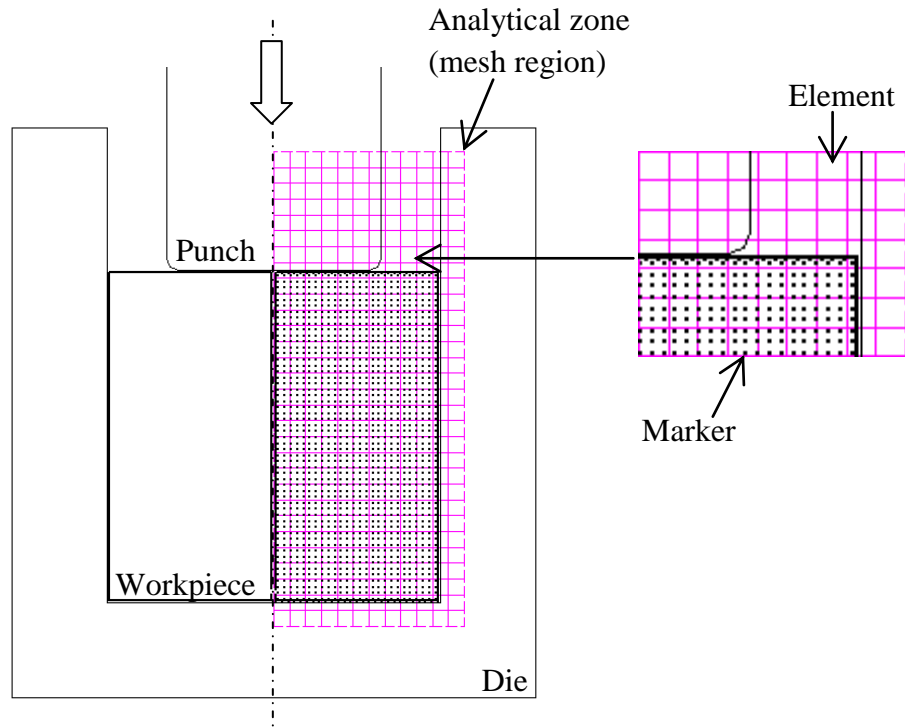


Figure 3.4: Defining analytical zone in backward extrusion using Eulerian mesh.

### 3.2.1.2 Searching the Tool Boundaries

Figure 3.5 shows the procedures of searching boundary line before each incremental deformation. For example, the punch in Fig. 3.5 does not located exactly on the lines of elements. Starting from centre of the punch, the nearest nodal point to the punch labeled with 1 in Fig. 3.5(a) is identified. Then, the nodal point will be shifted to the edge of the tool represented as 1' in Fig. 3.5(b). Nodal point 2 is then shifted to position 2'. The line between nodal points 1' and 2' is a boundary line labeled with (1) as shown in Fig. 3.5(k). The remaining boundary lines will be labeled in bracket according to this order. Nodal point 4 in Fig. 3.5(d) is shifted twice to form a better boundary line at the fillet region of punch as shown in Fig. 3.5(e) and (f). Each element will only consists four nodal points and the repositioning processes are continued until the boundary lines for every tool and dies are completely defined in each step. Point 1',2',3',4'',5',6',7',8' and 9' in Fig. 3.5(k) is the defined boundary line.

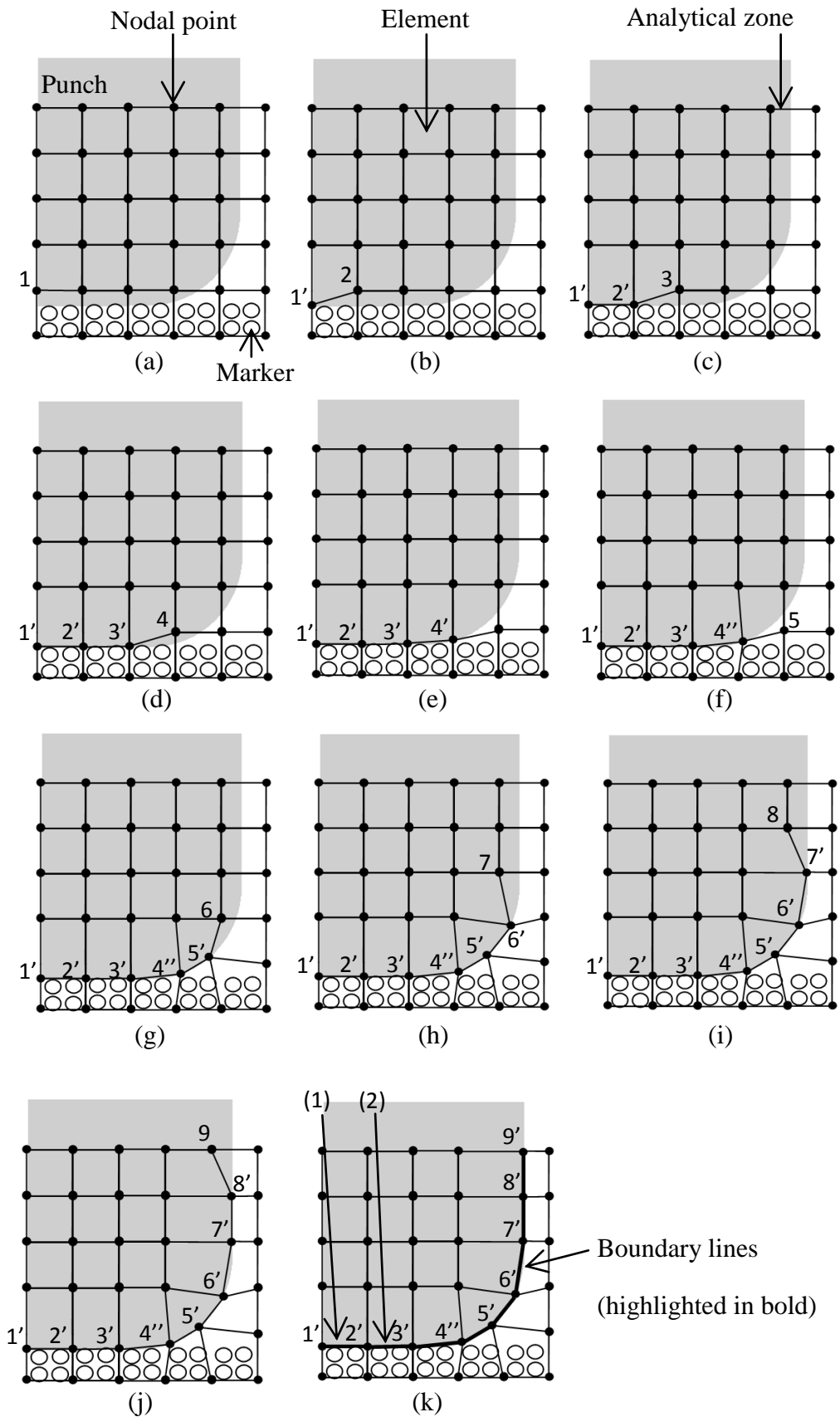


Figure 3.5: Searching for boundary lines in Eulerian mesh.

### 3.2.1.3 Before Solving the Matrix

After searching the boundary lines on the tools and dies, the average equivalent strain  $\bar{\varepsilon}_{ave}$  of each element were calculated from markers. For an example, if there are four markers inside an element, the average equivalent strain of the four markers will be distributed into nodal points based on the coordinate of the markers with respect to nodal points within the same element.

Then, the average flow stress  $\bar{\sigma}_{ave}$  of each element will be determined by using;

$$\bar{\sigma}_{ave} = F \bar{\varepsilon}_{ave}^n \dot{\varepsilon}_{ave}^m \quad (3.4)$$

where  $F$  is magnitude of flow stress,  $n$  is work hardening exponent and  $m$  is strain rate sensitivity.

Trial equivalent strain rate  $\dot{\varepsilon}$  of each element will be calculated from velocities of nodal points  $u_e$  using Eq. (3.3).

### 3.2.1.4 Constructing and Solving the Matrix

To obtain the velocity field, strain rate in each element was related by the velocities of nodal points;

$$\{\dot{\varepsilon}_0\} = [B_0]\{u_{e0}\} \quad (3.5)$$

where subscript 0 represents the beginning of each deformation step and  $[B_0]$  expressed by the coordinates of nodal points.

Stress within the element was related to nodal velocities by combining Eq. (3.2) and Eq. (3.5);

$$\{\sigma_0\} = \frac{\bar{\sigma}_0}{\dot{\varepsilon}_0(u_{e0})} [D][B_0]\{u_{e0}\} \quad (3.6)$$

Nodal forces of an element with volume  $V_e$  was expressed by the stress within the element;

$$\{P_0\} = \int_{V_e} [B_0]^T \{\sigma_0\} dV \quad (3.7)$$

Nodal forces of an element were related to nodal velocities by combining Eq. (3.6) and Eq. (3.7);

$$\{P_0\} = \int_{V_e} \frac{\bar{\sigma}_0}{\dot{\varepsilon}_0} [B_0]^T [D][B_0]\{u_{e0}\} dV = [K_0]\{u_{e0}\} \quad (3.8)$$

By considering the equilibrium of nodal forces at each nodal point, the following equation could be derived;

$$\sum^{\text{Element}} \{P_0\}_i = \begin{cases} F_i & (\text{on surface}) \\ 0 & (\text{in material}) \end{cases} \quad (3.9)$$

Iterative procedure without partial differential was used to approximate Eq. (3.8) and Eq. (3.9) to linear simultaneous equations;

$$[K_0]^{n-1}\{u_{e0}\}^n = \{F\}^{n-1} \quad (3.10)$$

where  $n$  is the number of iteration.

### 3.2.1.5 After Solving the Matrix

After solving the matrix, strains  $\{\varepsilon\}$ , stresses  $\{\sigma\}$ , equivalent strain rates  $\{\dot{\varepsilon}\}$ , and equivalent strains  $\{\bar{\varepsilon}\}$  for element will be updated. Then, velocities  $u_m$  and equivalent strain  $\bar{\varepsilon}_m$  of each marker inside the element will be calculated base on the coordinate of markers with respect to the nodal points in same element. Then, the tool was moved at  $\Delta t$  and  $\Delta$  step. The whole process was repeated again from searching and defining the new boundary lines in the next incremental step.

Element with no marker was omitted automatically to reduce the size of matrix for FEM analysis. Thus, the variables could be reduced and the computational time was shortened in solving Eq. (3.2).

## CHAPTER 4

### METHODOLOGY

#### 4.1 Introduction

The flow of this research was divided into 6 steps as shown in Fig. 4.1. Mainly, it was under two main categories which were experiments and simulations. Each step listed in Fig. 4.1 will be discussed in this chapter.

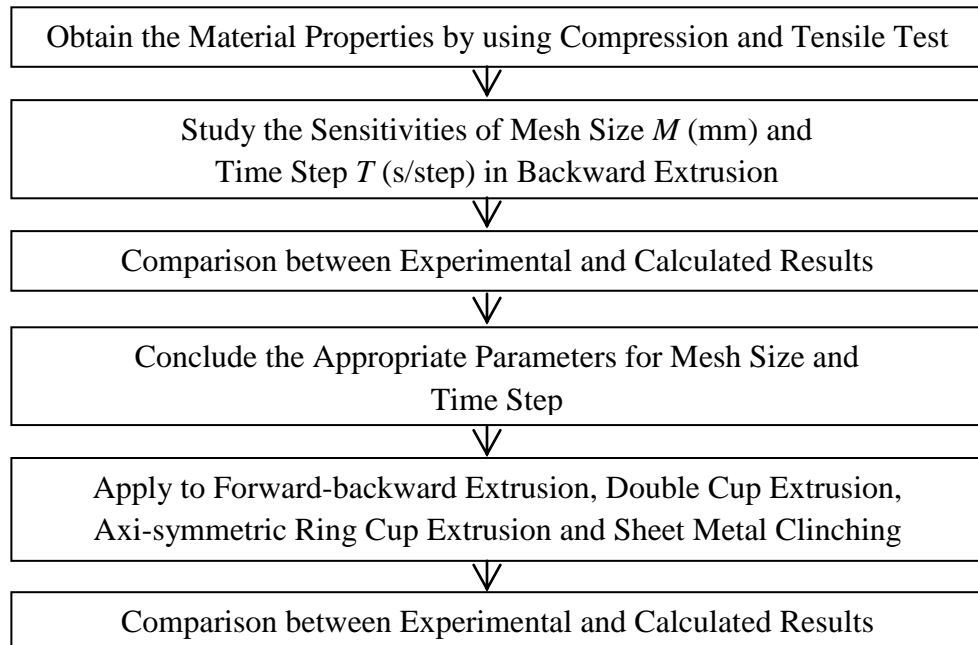


Figure 4.1: Flow of research.

## 4.2 Material Property

Material property is essential input for simulation because it will directly affect the accuracy of the simulation results. Compression tests and tensile tests were conducted to find the material properties for aluminium billet and steel metal sheet.

For extrusion process, compression test was used to collect engineering stress and engineering strain data. Firstly, aluminium billet with diameter to height ratio of 1:1 was placed on metal plate of universal testing machine. The billet was aligned on the center as shown in Fig. 4.2. Top and bottom surfaces of the billet were wrapped with Teflon tape to minimize the bulging effect. Bulging effect will reduce the accuracy of the data due to the irregular diameter after the deformation. Load was applied on the billet until it was deformed to half of its height. Data of engineering stress and strain was collected and converted to true stress and true strain. The flow stress curve for aluminium billet was calculated.

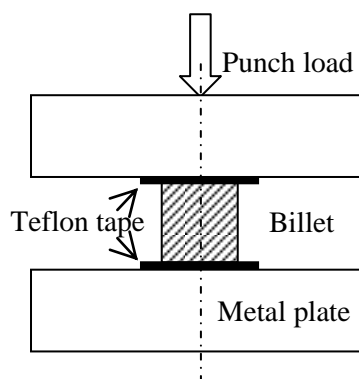


Figure 4.2: Compression test.

For sheet metal clinching, uniaxial tensile test was carried out on the same universal testing machine. Steel metal sheet as shown in Fig. 4.3 was pulled until fracture and the data for engineering stress and strain were collected and converted to true stress and true strain. The flow stress of the material was calculated.

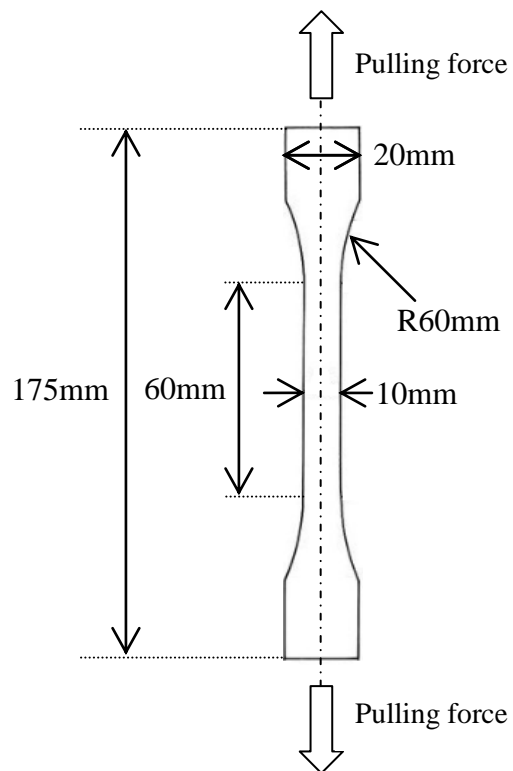


Figure 4.3: Tensile test for steel metal sheet.

Material properties and working conditions for aluminium billet and steel metal sheet are listed in the Table 4.1.

Table 4.1: Material properties and working conditions for the simulation.

Specimen material	Aluminium billet for extrusion	Steel metal sheet for clinching
Dimension of specimen (mm)	φ14 x 14	100 x 20 x 1.1
Lubricant	Mechanical oil	Without lubricant
Flow stress curve (MPa)	$\bar{\sigma} = F\bar{\varepsilon}^n$ $F = 415.16$ $n = 0.082$	$\bar{\sigma} = F\bar{\varepsilon}^n$ $F = 507$ $n = 0.32$

From the table above, flow stress equation is;

$$\bar{\sigma} = F\bar{\varepsilon}^n \quad (4.1)$$

Where  $\bar{\sigma}$  is equivalent stress,  $F$  is magnitude of flow stress,  $\bar{\varepsilon}$  is equivalent Strain and  $n$  is work hardening exponent.

Engineering stress  $\sigma_E$  and engineering strain  $\varepsilon_E$  obtained from compression and tensile test were converted to true stress  $\sigma_T$  and true strain  $\varepsilon_T$  using the following equations;

$$\sigma_T = \sigma_E(1 - \varepsilon_E) \quad (4.2)$$

$$\varepsilon_T = \ln(1 - \varepsilon_E) \quad (4.3)$$

Where  $\sigma_T$  is true stress,  $\sigma_E$  is engineering stress,  $\varepsilon_T$  is true strain and  $\varepsilon_E$  is engineering strain.

Then, true stress and true strain were converted into natural logarithm form and  $\ln \sigma_T$  versus  $\ln \varepsilon_T$  curve was plotted. A linear equation was obtained from the plastic region on  $\ln \sigma_T$  versus  $\ln \varepsilon_T$  curve;

$$\ln \sigma_T = m \ln \varepsilon_T + c \quad (4.4)$$

Where  $m$  is the gradient and  $c$  is the constant intersect on Y-axis.

In order to retrieve the value of magnitude of flow stress  $F$  and work hardening exponent  $n$ , Eq. (4.1) was converted into natural logarithm form and compared with Eq. (4.4). As a result;

$$F = c$$

$$n = m$$

### 4.3 Extrusions and Sheet Metal Clinching

Five types of metal forming processes such as backward extrusion, forward-backward extrusion, double cup extrusion, axi-symmetric ring cup extrusion and sheet metal clinching were conducted in the laboratory on the universal testing machine as shown in Fig. 4.4.

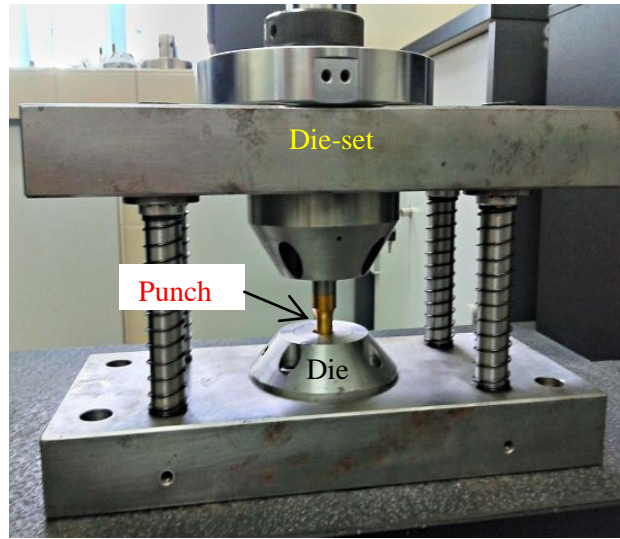


Figure 4.4: Tooling setup for extrusion processes.

Different dies and punches were inserted in the holder to suit the metal forming processes mentioned above. Data of punch load (kN) and punch stroke (mm) for all the 4 types of extrusions and sheet metal clinching were collected and compared with simulation results.

### 4.3.1 Extrusions

Different punches were used for different extrusions and the dimension of billets was  $\phi 14 \times 14$  mm. Mechanical oil was chosen as the lubricant for the extrusion processes. The well machined aluminium billet was put inside the die and the punch load was exerted on the billet until the punch stroke exceeded half of the billet's height. Then, the extrusion process was completed and stopped.

Figures from Fig. 4.5 to Fig 4.8 show the shape of the billets and dies at the beginning and end of all the different extrusion processes. In addition, the parameters and dimension of punches, dies and billet were listed in the figures accordingly.

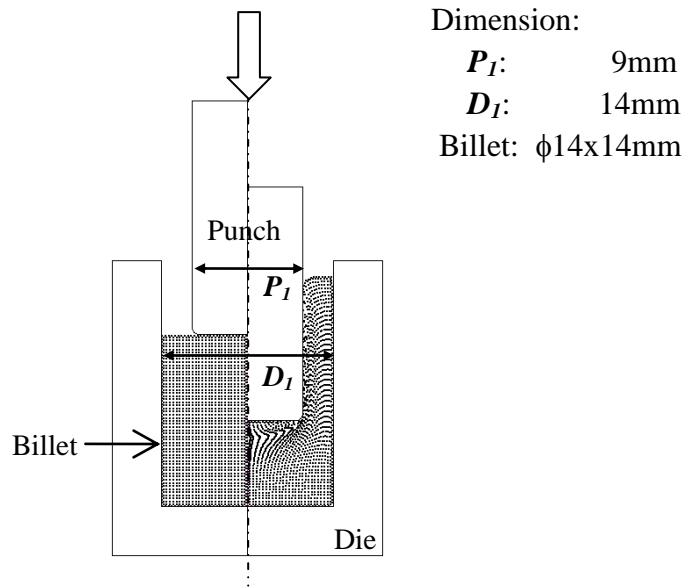


Fig. 4.5: Backward extrusion.

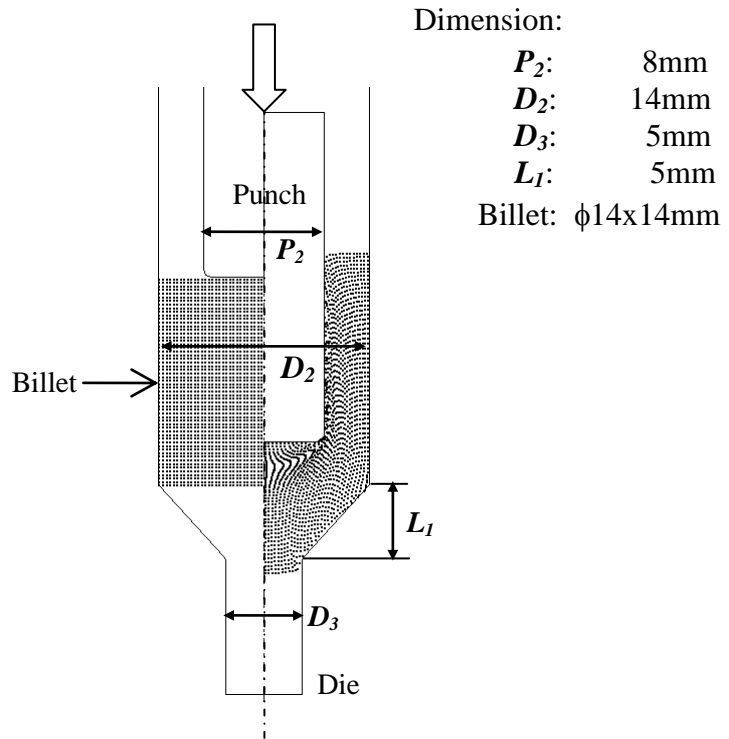


Fig. 4.6: Forward-backward extrusion.

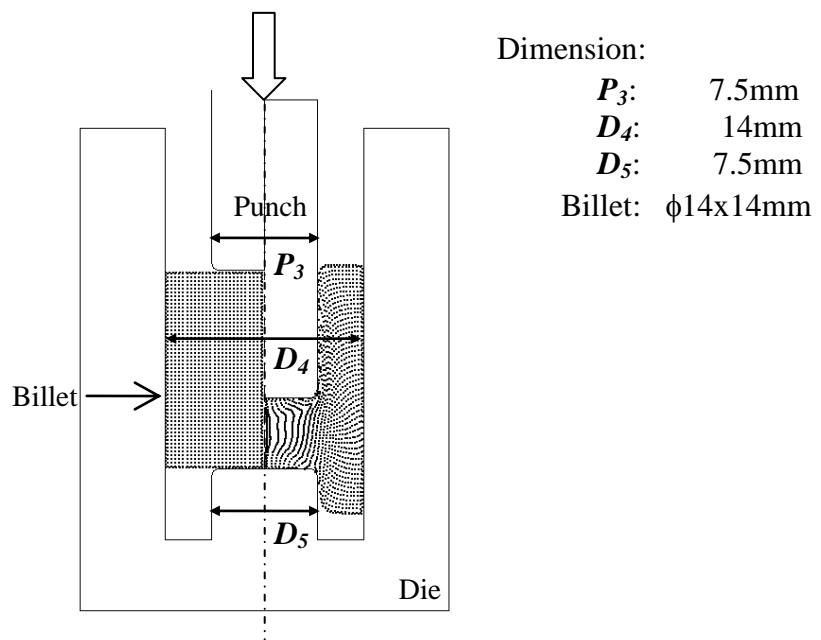


Fig. 4.7: Double cup extrusion.

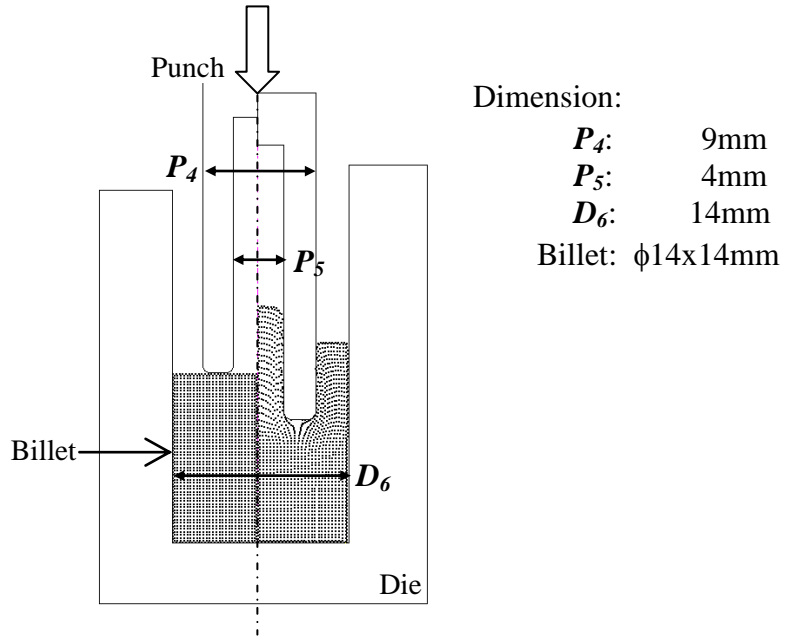


Fig. 4.8: Axi-symmetric ring cup extrusion.

#### 4.3.2 Sheet Metal Clinching

Sheet metal clinching is a joining method. Two layers of sheet metal blank were put on top of the lower die shown in Fig.4.9. Punch load was exerted on top of the center of blank. The shape of the lower die enabled the two layers of sheet metal to form an interlock and produced an axi-symmetrical joint.

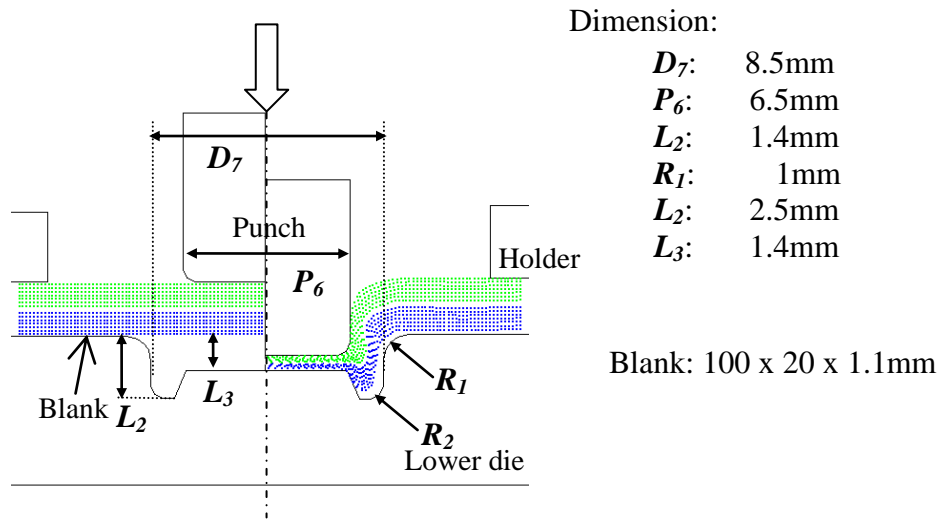


Fig. 4.9: Sheet metal clinching.

#### 4.4 FEM Simulation

FEM simulation was divided into three steps as shown in Fig. 4.10.

Firstly, the parameter and dimension of the workpiece, tools and mechanical properties were defined in the preprocessor phase. Then, the calculation will be done under solver mode. Lastly, the graphical simulation result will be shown in postprocessor stage.



Fig. 4.10: Stages in FEM simulation

In preprocessor stage, two dimensional models of tools and workpiece were drawn inside a graphic user interface. Only half of the tools and workpiece were modeled because everything was defined under axi-symmetric model. Followed by is the selection of material. Since the aluminium alloy and steel sheet used in the study were not included in the material database, the values of flow stress  $F$  and work hardening exponent  $n$  were calculated using the data from compression and tensile test as shown in Table. 4.1.

Then, an analytical zone was defined around the workpiece with Eulerian meshing. In order to study the sensitivities of mesh size  $M$  (mm) and time step  $T$  (s/step), the chosen range was shown in Table 4.2.

Table 4.2: Parameters for mesh size and time step.

<b>Mesh Size <math>M</math> (mm)</b>	0.3, 0.5 and 0.7
<b>Time Step <math>T</math> (s/step)</b>	0.005, 0.05 and 0.5

With maximum number of 1600 nodal points, elements and markers, simulation parameters shown in Table 4.2 were applied on the simulation of backward extrusion to study the sensitivities of mesh size and time step. Punch load and punch stroke obtained from simulations and experiments were compared. Besides, the computational time taken and extruded shapes of backward extrusion with different mesh sizes and time steps were considered as well to find the appropriate parameters for mesh size and time step in Eulerian mesh.

Hence, the appropriate parameters for mesh size and time step were applied to forward-backward extrusion, double cup extrusion, axi-symmetric ring cup extrusion and sheet metal clinching in simulations. Simulation and experimental results of punch load, punch stroke and extruded shapes from all the metal forming processes conducted in this study were collected, compared and discussed.

## **CHAPTER 5**

### **VALIDATION BETWEEN SIMULATION AND EXPERIMENTAL RESULT**

#### **5.1 Introduction**

Metal forming operations such as backward extrusion, forward-backward extrusion, axi-symmetric ring cup extrusion, double cup extrusion and sheet metal clinching were conducted on universal testing machine and the processes were simulated using rigid-plastic finite element by applying Eulerian meshing scheme. Punch load and punch stroke for both experimental and calculated results were collected and plotted into graphs for comparison purpose.

Besides, mesh size  $M$  (mm) and time step  $T$  (s/step) were the parameters chosen to study the effectiveness of Eulerian meshing method in bulk metal forming and sheet metal clinching processes.

## 5.2 Backward Extrusion

In order to deploy a mesh region of 14x18mm to cover the deformation of workpiece in backward extrusion with maximum of 1600 nodal points and 1600 elements, the optimum range for mesh size was from 0.3mm to 0.7mm. The sensitivities of mesh size  $M$  and time step  $T$  were studied in the simulation of backward extrusion.

Mesh size  $M$  was represented by the width or height of an element as shown in Fig 5.1. Three types of mesh size, i.e.,  $M = 0.3\text{mm}$ ,  $0.5\text{mm}$  and  $0.7\text{mm}$  were considered in the simulation to study the sensitivities are shown in Fig 5.2. In addition, three time step, i.e.,  $T = 0.005\text{s/step}$ ,  $0.05\text{s/step}$  and  $0.5\text{s/step}$  were chosen in this study as well.

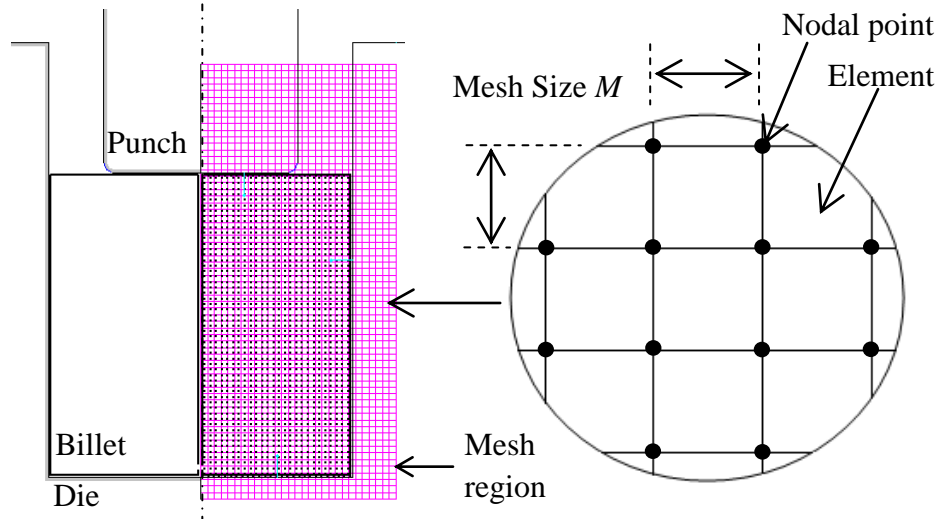
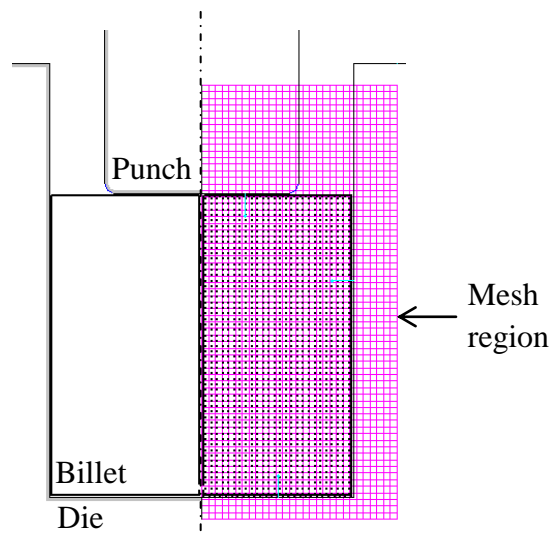
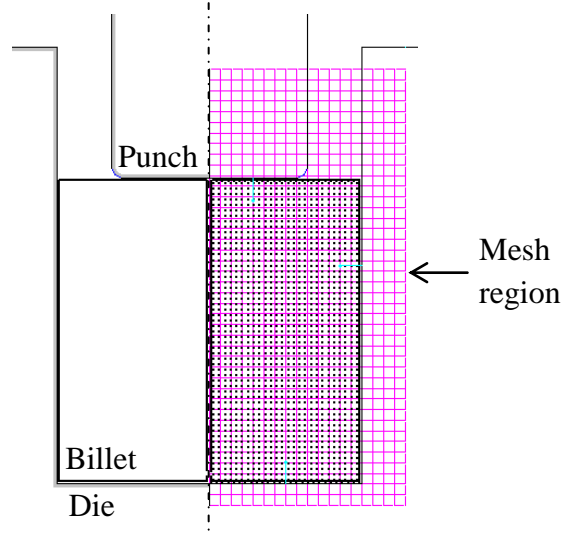


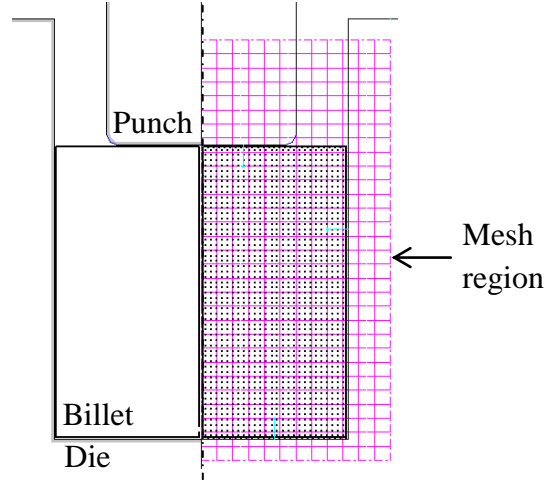
Figure 5.1: Mesh size.



(a) Mesh size  $M = 0.3\text{mm}$



(b) Mesh size  $M = 0.5\text{mm}$



(c) Mesh Size  $M = 0.7\text{mm}$

Figure 5.2: Different mesh sizes  $M$  in backward extrusion.

### 5.2.1 Sensitivity of Mesh Size

The study of sensitivity for mesh size was defined into 3 conditions and each condition was carried out with a fixed time step  $T$  and three different mesh sizes  $M$  as shown in Fig. 5.1. The calculated and experimental punch load curves were plotted into graphs for comparison purposes.

Table 5.1: Conditions used to study the sensitivity of mesh size in backward extrusion.

Condition	Time Step $T$ (s/step)	Mesh Size $M$ (mm)
1	0.005	0.3, 0.5 and 0.7
2	0.05	
3	0.5	

In non-linear numerical calculation, the convergence procedure in the non-steady state boundary condition in finite element method creates fluctuations of value for the punch load. In order to have a proper comparison with the experimental results, the punch load data were approximated into smooth curves using polynomial equations as shown in Fig. 5.3. Since rigid-plastic finite element method is applied in this study, the early stage of elastic deformation is not taken into consideration. Therefore, the deviations of punch loads at the early stage can be seen but ignored in the comparisons.

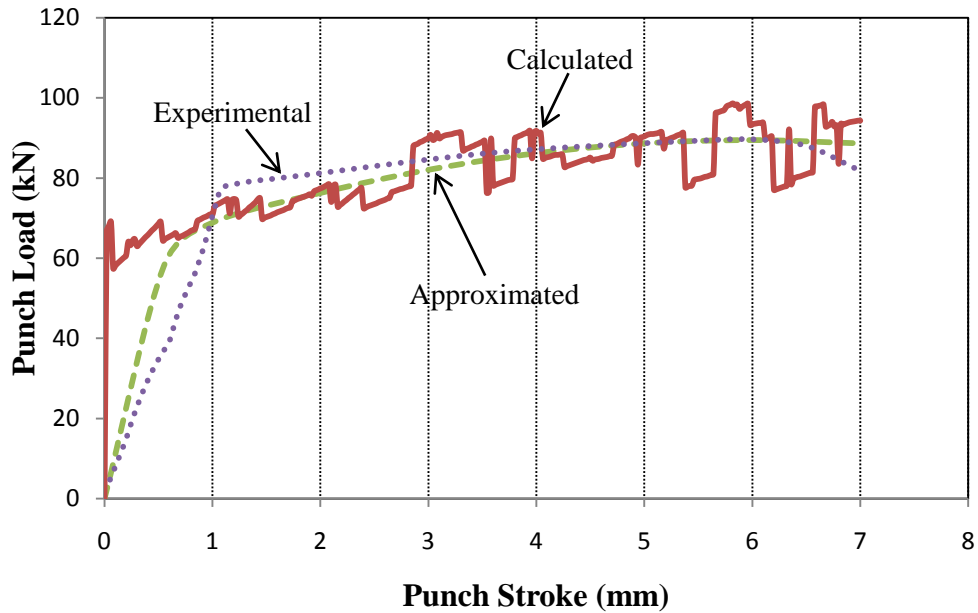


Figure 5.3: Polynomial approximation of punch load curve.

(time step  $T = 0.005\text{s}/\text{step}$  and mesh size  $M = 0.5\text{mm}$ )

To study the sensitivity for mesh size  $M$  and time step  $T$ , six calculated and experimental punch loads for punch stroke at 2, 3, 4, 5, 6 and 7mm as shown in Fig 5.3 were referred to examine the percentage errors. Punch loads at 1mm of punch stroke were omitted because early stage of elastic deformation was not taken into consideration in this study.

**5.2.1.1 Condition 1: Time Step  $T = 0.005\text{s}/\text{step}$  by varying  
Mesh Sizes  $M = 0.3, 0.5$  and  $0.7\text{mm}$**

The extruded shapes obtained from condition 1 were compared in Fig. 5.4. The final shapes obtained by  $M = 0.3$  and  $0.5\text{mm}$  were identical, however the extruded shape obtained by  $M = 0.7\text{mm}$  was different at the top left and right corners where the inner height was significantly lower than the outer height as shown in Fig. 5.4 (c). Higher punch loads by  $M = 0.7\text{mm}$  as shown in Fig. 5.5 caused the material flow of inner surface slower.

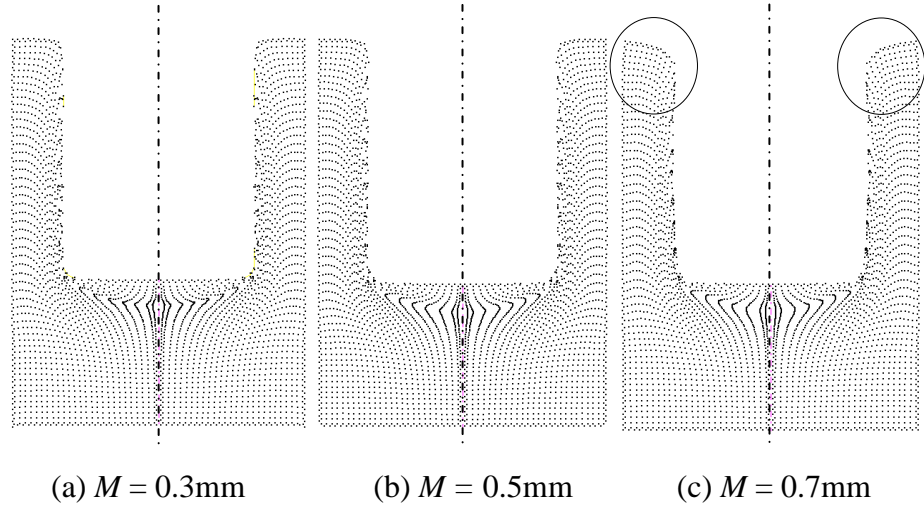


Figure 5.4: Extruded shapes for different mesh sizes in backward extrusion at time step =  $0.005\text{s}/\text{step}$ .

Calculated punch load curves were plotted in Fig. 5.5 and compared with experimental curve, punch loads for  $M = 0.3\text{mm}$  were lowest, followed by  $M = 0.5\text{mm}$  which was closest to experimental result and punch loads for  $M = 0.7\text{mm}$  remained as the highest. Average percentage errors of six punch loads for calculated and experimental results at punch stroke of 2, 3, 4, 5, 6, and

7mm were tabulated in Table 5.2. Calculated punch loads for  $M = 0.5\text{mm}$  achieved the lowest average percentage error.

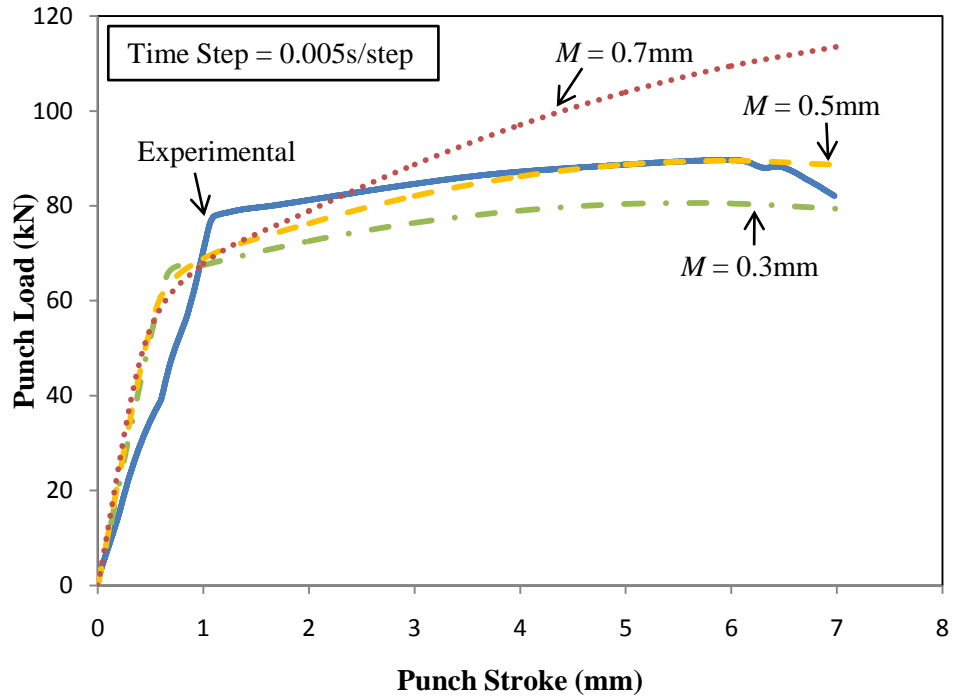


Figure 5.5: Comparison of punch load curves between experiment and calculations for different mesh sizes in backward extrusion at time step = 0.005s/step.

Table 5.2: Comparison of punch loads between experiment and calculations for different mesh sizes in backward extrusion at time step = 0.005s/step.

Stroke (mm)	Mesh Size (mm)	Time Step = 0.005 s/step		
		0.3	0.5	0.7
	Experimental Punch Load (kN)	Calculated Punch Load (kN)		
2	81.22	72.58	76.28	78.93
3	84.61	76.40	82.06	88.69
4	87.17	78.99	86.18	97.03
5	88.69	80.36	88.66	103.95
6	89.65	80.48	89.48	109.43
7	82.10	79.38	88.65	113.49
Average Percentage Error (%)		9	3	16

### 5.2.1.2 Condition 2: Time step $T = 0.05\text{s}/\text{step}$ by varying

#### Mesh Sizes $M = 0.3, 0.5$

At higher time step, the sensitivity of mesh sizes was studied. Extruded shapes obtained from three different mess sizes were shown in Fig. 5.6. The extruded shapes for  $M = 0.3$  and  $0.5\text{mm}$  were similar but the top left and right corners for  $M = 0.7\text{mm}$  again showed differences.

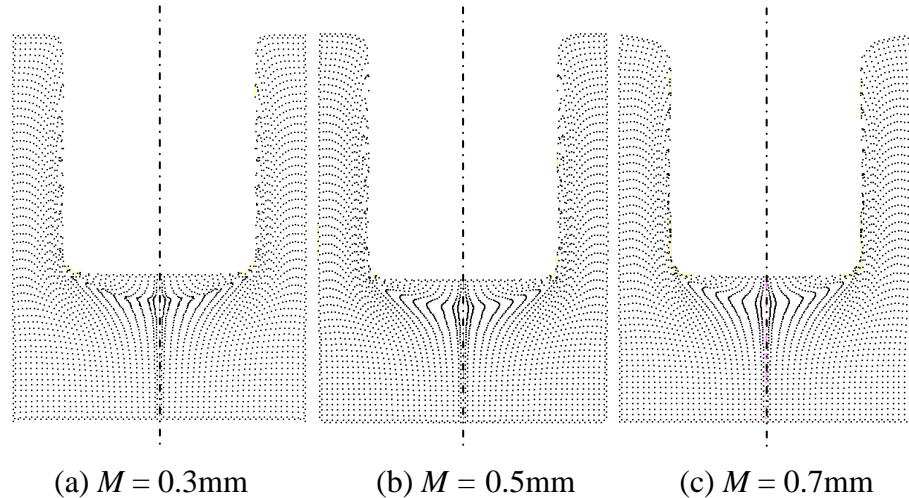


Figure 5.6: Extruded shapes for different mesh sizes in backward extrusion at time step =  $0.05\text{s}/\text{step}$ .

Punch load curves for  $M = 0.3$  and  $0.5\text{mm}$  were closer to experimental curve while the  $M = 0.7\text{mm}$  curve showed highest deviation of 17% when compared to experimental results as shown in Fig. 5.7 and Table 5.3.

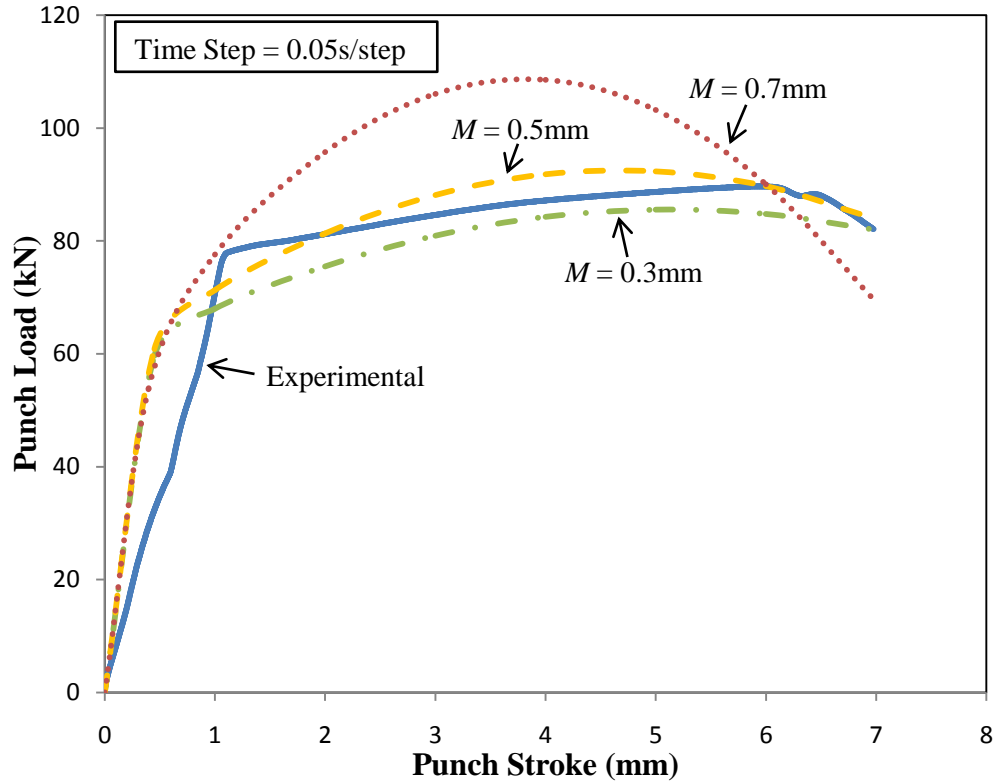


Figure 5.7: Comparison of punch load curves between experiment and calculations for different mesh sizes in backward extrusion at time step = 0.05s/step.

Table 5.3: Comparison of punch loads between experiment and calculations for different mesh sizes in backward extrusion at time step = 0.05s/step.

Stroke (mm)	Mesh Size (mm)	Time Step = 0.05 s/step			
		0.3	0.5	0.7	
		Experimental Punch Load (kN)	Calculated Punch Load (kN)		
2		81.22	75.49	81.30	95.72
3		84.61	80.90	88.14	106.03
4		87.17	84.25	91.82	108.52
5		88.69	85.54	92.34	103.20
6		89.65	84.77	89.70	90.06
7		82.10	81.94	83.90	69.11
Average Percentage Error (%)			4	3	17

### 5.2.1.3 Condition 3: Time step $T = 0.5\text{s}/\text{step}$ by varying

#### Mesh Sizes $M = 0.3, 0.5$ and $0.7\text{mm}$

At highest time step  $T = 0.5\text{s}/\text{step}$  in this study, the markers in the inner surface of extruded shapes from all mesh sizes were in scattered form as shown in Fig. 5.8. The severity of distortion for the markers did improve with lower mesh size but it was still not acceptable to compare with experimental result. Calculated punch load curves showed ascending order from  $M = 0.3$  to  $0.7\text{mm}$  as shown in Fig. 5.9. Average percentage errors for all mesh sizes at  $T = 0.5\text{s}/\text{step}$  are the highest when compared with lower time steps and range from 6 to 18 % as shown in Table 5.4.

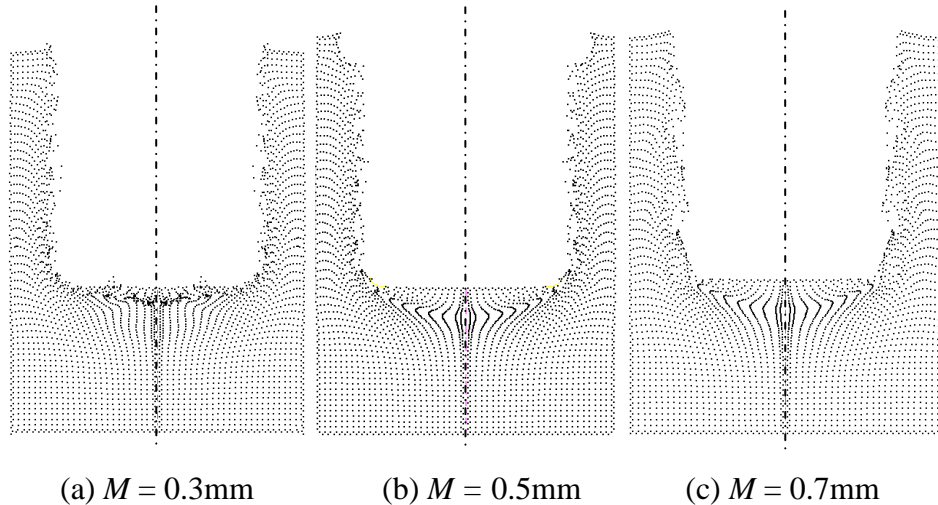


Figure 5.8: Extruded shapes for different mesh sizes in backward extrusion at time step =  $0.5\text{s}/\text{step}$ .

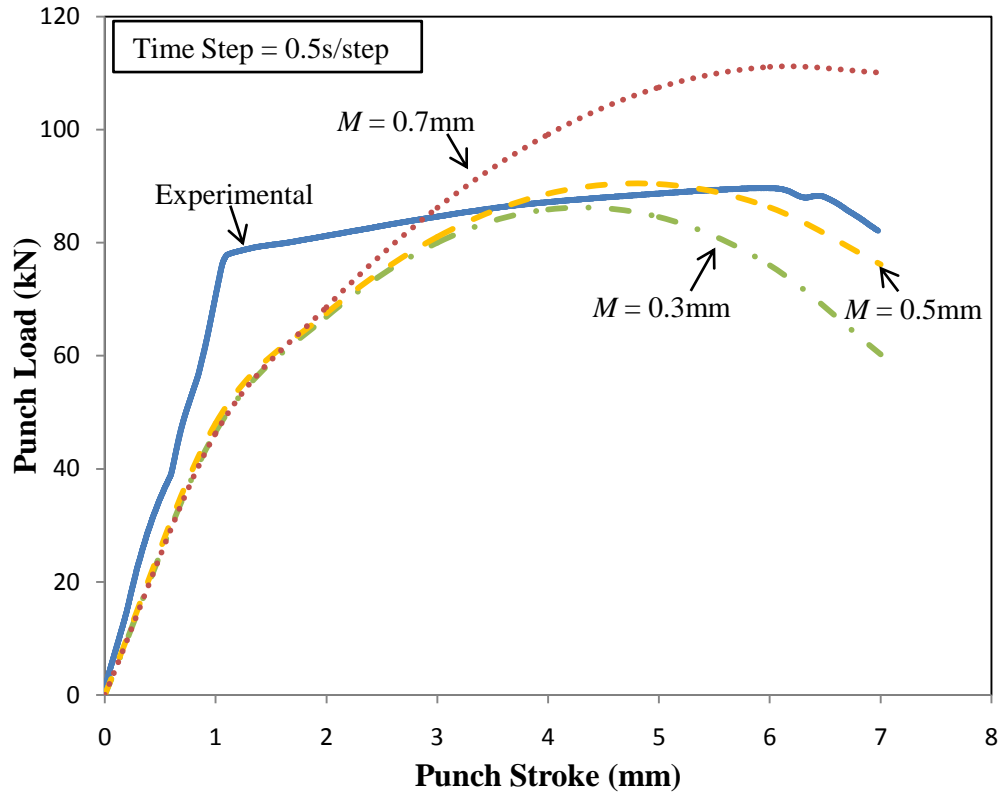


Figure 5.9: Comparison of punch load curves between experiment and calculations for different mesh sizes in backward extrusion at time step = 0.5s/step.

Table 5.4: Comparison of punch loads between experiment and calculations for different mesh sizes in backward extrusion at time step = 0.5s/step.

Stroke (mm)	Mesh Size (mm)	Time Step = 0.5 s/step		
		0.3	0.5	0.7
	Experimental Punch Load (kN)	Calculated Punch Load (kN)		
2	81.22	66.88	67.47	68.56
3	84.61	79.98	81.01	86.18
4	87.17	85.86	88.65	99.14
5	88.69	84.54	90.38	107.45
6	89.65	76.00	86.21	111.08
7	82.10	60.26	76.13	110.06
Average Percentage Error (%)		12	6	18

### 5.2.2 Sensitivity of Time Step

Simulation parameters were given in 3 conditions as shown in Table 5.5 with a fixed mesh size and three time steps to study the sensitivity of time step  $T$ . Calculated and experimental punch load curves were plotted into graphs, compared and discussed.

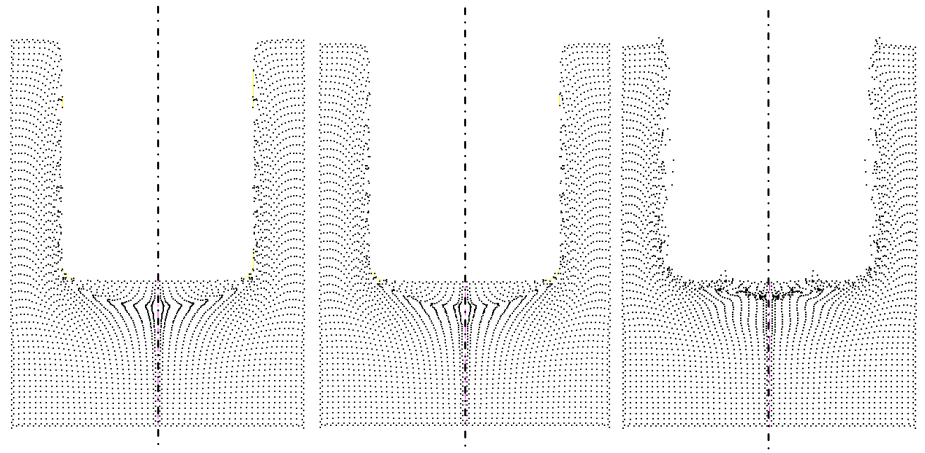
Table 5.5: Conditions used to study the effect of mesh size in backward extrusion.

Condition	Mesh Size $M$ (mm)	Time Step $T$ (s/step)
<b>1</b>	0.3	0.005, 0.05 and 0.5
<b>2</b>	0.5	
<b>3</b>	0.7	

#### 5.2.2.1 Condition 1: Mesh Size $M = 0.3\text{mm}$ by varying Time Steps

**$T = 0.005, 0.05 \text{ and } 0.5\text{s/step}$**

The markers were scattered around in the inner surface of the extruded shape for  $T = 0.5\text{s/step}$  while the shapes of the final product remained identical and similar for  $T = 0.005$  and  $0.05\text{s/step}$  as shown in Fig. 5.10. With smallest mesh size  $M = 0.3\text{mm}$  in this study, the accuracy of the punch load curves did not improve with lower time step  $T$  where the average percentage errors in Table 5.6 showed 12, 4 and 9% for  $T = 0.5, 0.05$  and  $0.005\text{ s/step}$  respectively. Calculated punch load curves for all the time steps  $T$  with mesh size  $M = 0.3\text{mm}$  were plotted in Fig. 5.11 and did not show any uniform pattern.



(a)  $T = 0.005\text{s}/\text{step}$       (b)  $T = 0.05\text{s}/\text{step}$       (c)  $T = 0.5\text{s}/\text{step}$

Figure 5.10: Extruded shapes for different time steps in backward extrusion at mesh size = 0.3mm.

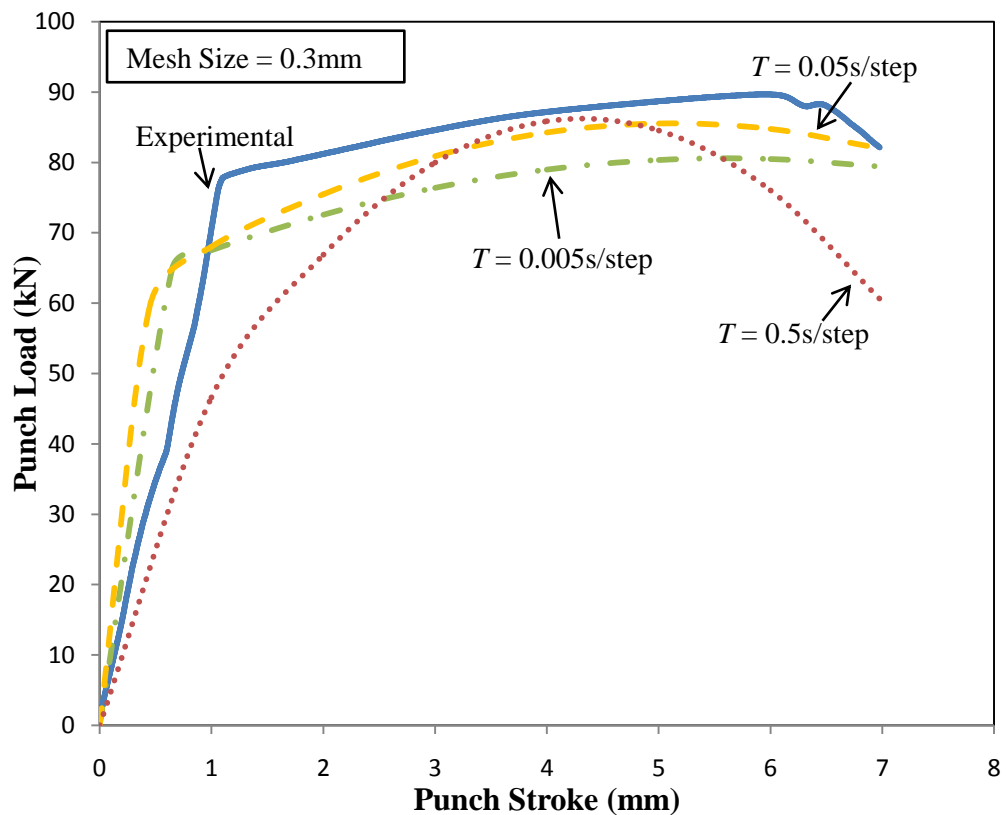


Figure 5.11: Comparison of punch load curves between experiment and calculations for different time steps in backward extrusion with mesh size = 0.3mm.

Table 5.6: Comparison of punch loads between experiment and calculations for different time steps in backward extrusion with mesh size = 0.3mm.

Stroke (mm)	Time Step (s/step)	Mesh Size = 0.3 mm		
		0.005	0.05	0.5
	Experimental Punch Load (kN)	Calculated Punch Load (kN)		
2	81.22	72.58	75.49	66.88
3	84.61	76.40	80.90	79.98
4	87.17	78.99	84.25	85.86
5	88.69	80.36	85.54	84.54
6	89.65	80.48	84.77	76.00
7	82.10	79.38	81.94	60.26
<b>Average Percentage Error (%)</b>		9	4	12

### 5.2.2.2 Condition 2: Mesh Size $M = 0.5\text{mm}$ by varying Time Steps

**$T = 0.005, 0.05 \text{ and } 0.5\text{s/step}$**

Same phenomena happened in extruded shape of  $T = 0.5\text{s/step}$  as shown in Fig. 5.12 (c), the markers within the inner surface were in scattered form when compared to lower time step with same mesh size. Although the parameter for time step  $T = 0.5\text{s/step}$  and mesh size  $M = 0.5\text{mm}$  did not show good extruded shape as mentioned above but the accuracy of punch loads obtained was the best when compared to others mesh sizes with same time step. Calculated punch load curves as shown in Fig. 5.13 were closer to experimental curve if compared to conditions 1 and 3 which means the average percentage error for all the time steps  $T$  with mesh size  $M = 0.5\text{mm}$  are the lowest.

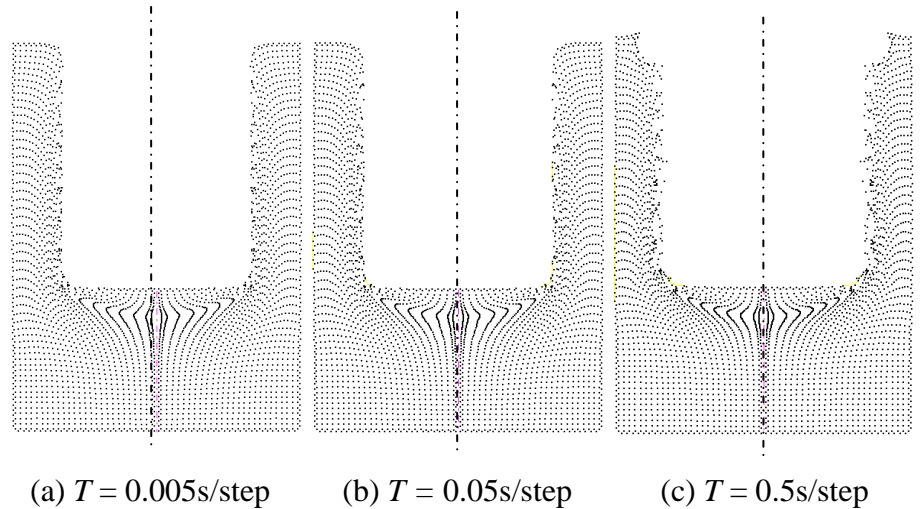


Figure 5.12: Extruded shapes for different time steps in backward extrusion at mesh size = 0.5mm

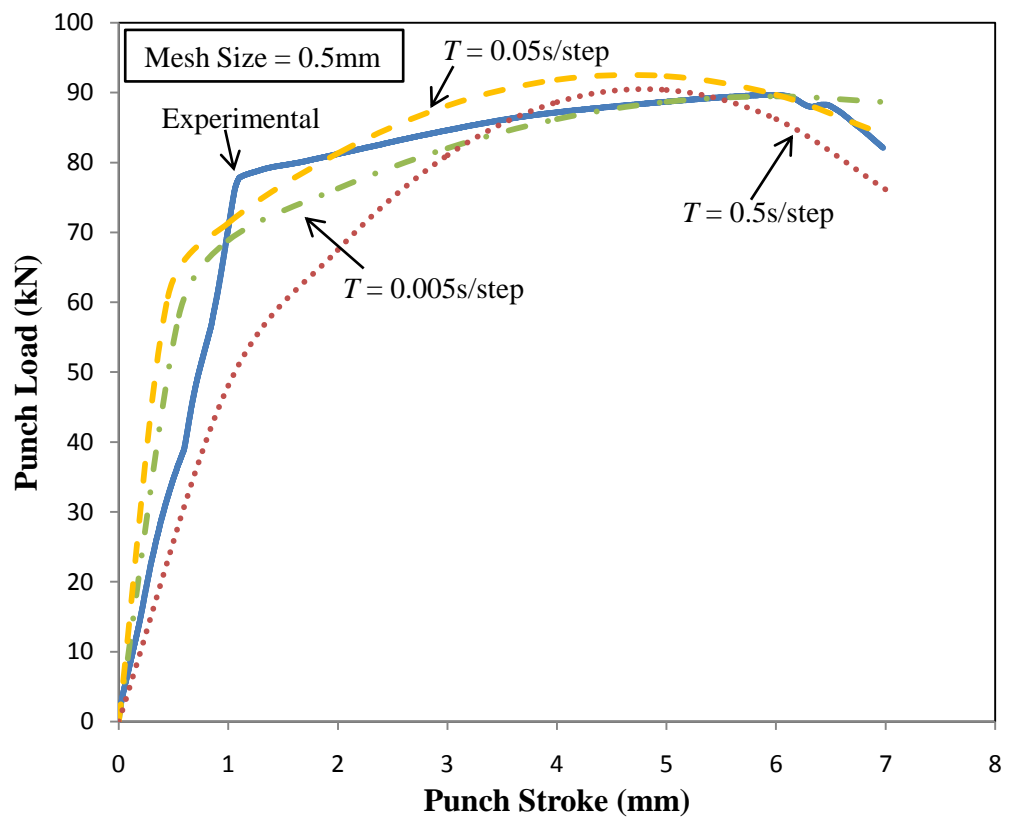


Figure 5.13: Comparison of punch load curves between experiment and calculations for different time steps in backward extrusion with mesh size = 0.5mm.

Table 5.7: Comparison of punch loads between experiment and calculations for different time steps in backward extrusion with mesh size = 0.5mm.

Stroke (mm)	Time Step (s/step)	Mesh Size = 0.5 mm		
		0.005	0.05	0.5
		Experimental Punch Load (kN)	Calculated Punch Load (kN)	
2	81.22	76.28	81.30	67.47
3	84.61	82.06	88.14	81.01
4	87.17	86.18	91.82	88.65
5	88.69	88.66	92.34	90.38
6	89.65	89.48	89.70	86.21
7	82.10	88.65	83.90	76.13
<b>Average Percentage Error (%)</b>		3	3	6

### 5.2.2.3 Condition 3: Mesh Size $M = 0.7\text{mm}$ by varying Time Steps

$$T = 0.005, 0.05 \text{ and } 0.5\text{s/step}$$

From the comparisons for sensitivity of mesh size, the top left and right corners on the extruded shapes of mesh size  $M = 0.7\text{mm}$  were found to be different from lower mesh sizes. Calculated punch load curves for three time steps showed high deviation as seen in Fig. 5.15. In addition, the average percentage errors in Table 5.8 ranged from 16 to 18% which were the highest values obtained in all the conditions. It was clearly showed that, no significant improvement could be done in term of better extruded shape and better accuracy of punch load curves when reducing the time step  $T$  at mesh size  $M = 0.7\text{mm}$ .

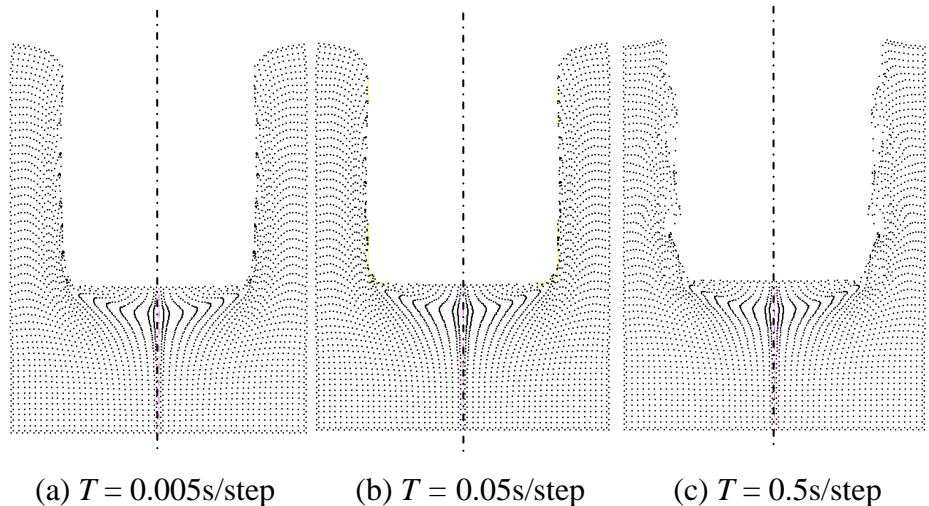


Figure 5.14: Extruded shapes for different time steps in backward extrusion with mesh size = 0.7mm.

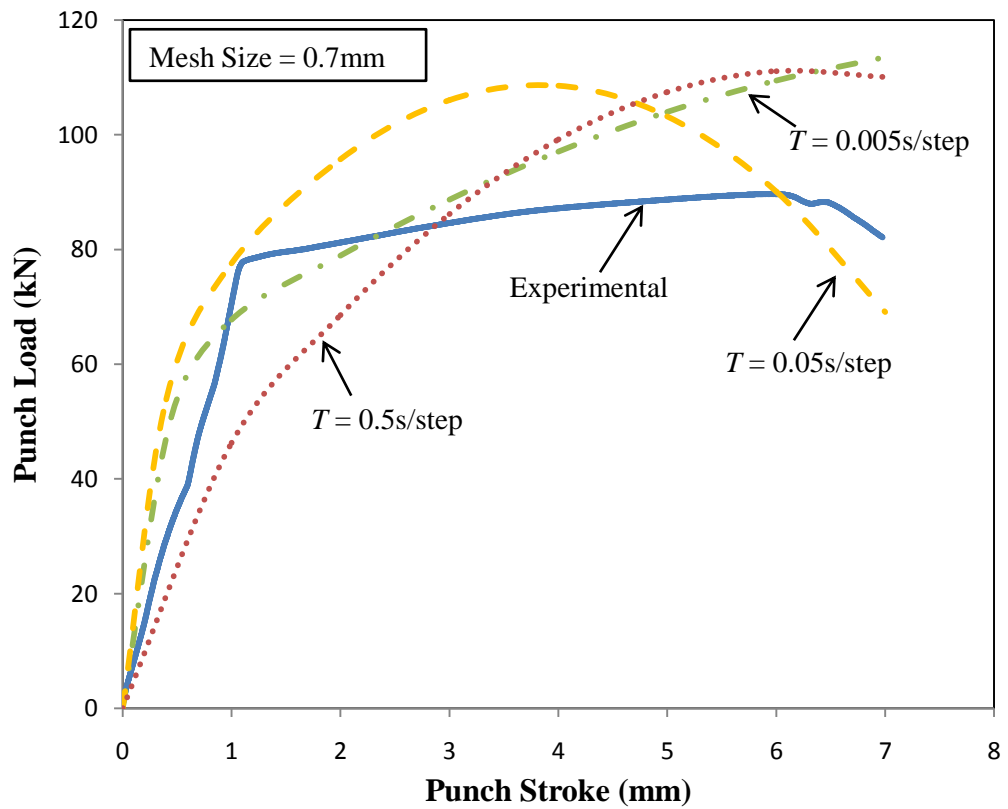


Figure 5.15: Comparison of punch load curves between experiment and calculations for different time steps in backward extrusion with mesh size = 0.7mm.

Table 5.8: Comparison of punch loads between experiment and calculations for different time step in backward extrusion with mesh size = 0.7mm.

Stroke (mm)		Mesh Size = 0.7 mm		
	Time Step (s/step)	0.005	0.05	0.5
	Experimental Punch Load (kN)	Calculated Punch Load (kN)		
2	81.22	78.93	95.72	68.56
3	84.61	88.69	106.03	86.18
4	87.17	97.03	108.52	99.14
5	88.69	103.95	103.20	107.45
6	89.65	109.43	90.06	111.08
7	82.10	113.49	69.11	110.06
<b>Average Percentage Error (%)</b>		16	17	18

### 5.2.3 Conclusion

Computational time required to solve the FEM calculation for all simulation parameters were recorded and tabulated in Table 5.9. Besides, the specification of the computer used in this study was listed in the same table as well. According to Table 5.9, finer mesh size and slower time step contributed to higher computational time while bigger mesh size and larger time step will speed out the calculation in solver stage.

Table 5.9: Computational time.

Specification of Computer			
Processor	Intel(R) Core(TM) i5 CPU M480 @ 2.67GHz		
RAM	4 GB		
		Mesh Size $M$ (mm)	
Time Step $T$ (s/step)	0.3	0.5	0.7
Computational Time (s)			
0.005	1572	960	297
0.05	100	46	19
0.5	12	5	2

Table 5.10: Percentage error for all simulation parameters.

Time Step $T$ (s/step)	Mesh Size $M$ (mm)		
	0.3	0.5	0.7
	Average Percentage Error (%)		
0.005	9	3	16
0.05	4	3	17
0.5	12	6	18

Mesh size  $M = 0.7\text{mm}$  contributed to the highest percentage errors for all the three time steps. Calculated punch load for  $M = 0.7\text{mm}$  curves were higher and extruded shapes showed slight difference especially on the top right and left corners due to the slower material flow in the inner surface of the workpiece. Boundary lines in larger mesh size were not fine enough to define a tool or die as shown in Fig. 5.16, therefore the accuracy of  $M = 0.7\text{mm}$  was affected.

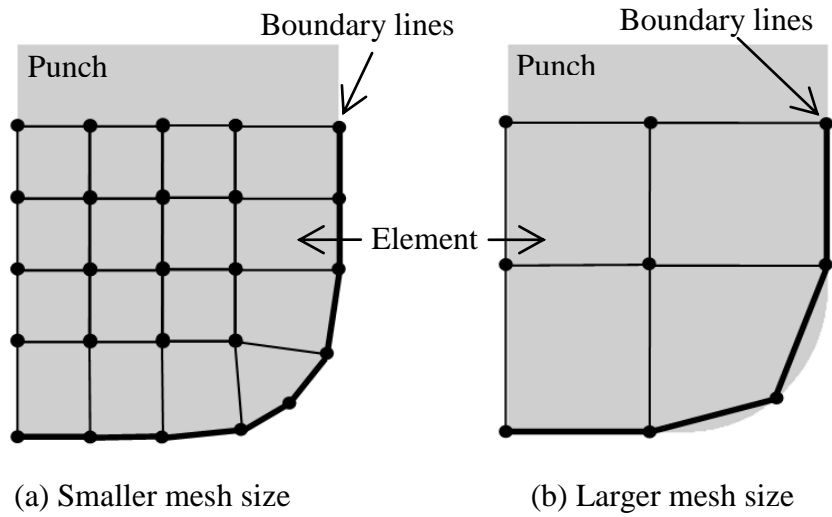


Figure 5.16: Boundary lines for different mesh size.

Theoretically, accuracy of the results will increase with finer mesh size but this did not happen on  $M = 0.3\text{mm}$  because the average percentage errors obtained were higher compared to  $M = 0.5\text{mm}$  as shown in Table 5.10. Since the difference between the value of mesh size  $M = 0.3\text{mm}$  and markers distance  $D = 0.25\text{mm}$  was very small, the probability of elements without marker as shown in Fig. 5.17 were higher. Therefore, element without marker will be omitted and treated as void. Thus, the results of punch load for  $M = 0.3\text{mm}$  were affected.

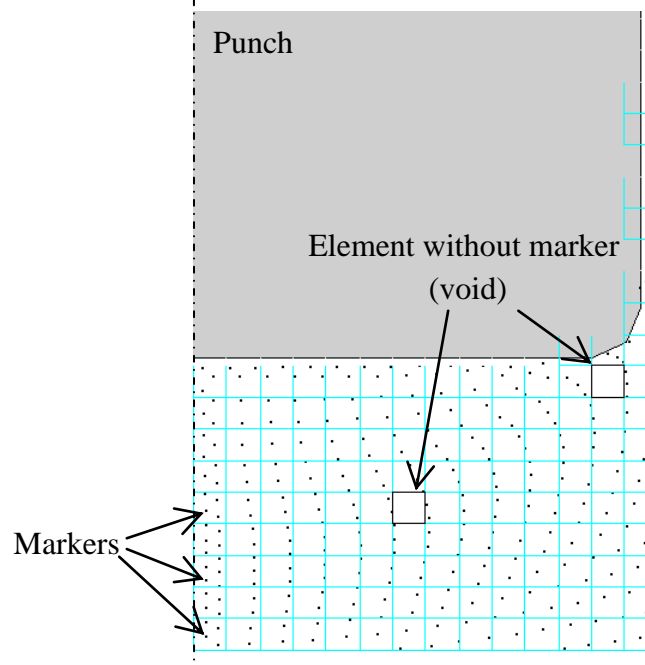


Figure 5.17: Element with no marker.  
(Mesh size  $M = 0.3\text{mm}$  and markers distance  $D = 0.25\text{mm}$ )

At time step  $T = 0.005\text{s}/\text{step}$ , the accuracy showed improvement from mesh size  $M = 0.7$  to  $0.5\text{mm}$  but drops again at  $M = 0.3\text{mm}$ . This was because the chances of forming voids in  $M = 0.3\text{mm}$  were higher. At highest time step  $T = 0.5\text{s}/\text{step}$ , the percentage errors were highest for all three mesh sizes as shown in Table 5.10.

With maximum of 1600 nodal points, 1600 elements and 1600 markers, the most appropriate simulation parameters were mesh size  $M = 0.5\text{mm}$  and time step  $T = 0.05\text{s}/\text{step}$  because it showed lowest percentage errors, good extruded shape and average computational time when compared to other simulation parameters. Thus simulation parameters for mesh size  $M = 0.5\text{mm}$  and time step  $T = 0.05\text{s}/\text{step}$  were applied to simulation of forward-backward extrusion, double cup extrusion, ring cup extrusion and sheet metal clinching.

Fig. 5.18 shows the side by side comparison of backward extrusion between experimental and calculation result. The extruded shapes were in good agreement.

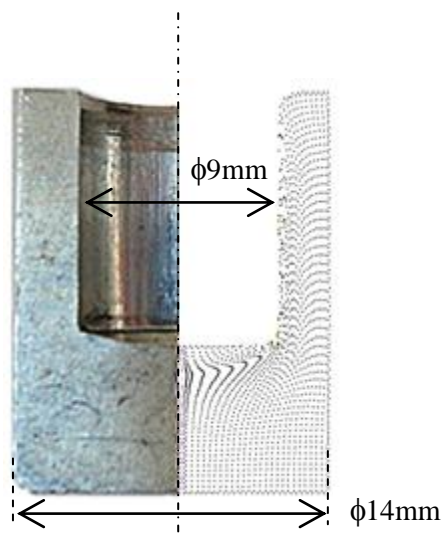


Figure 5.18: Comparison of extruded shape between experiment and calculation for backward extrusion  
(mesh size = 0.5mm and time step = 0.05s/step and experimental punch rate=2mm/min).

### 5.3 Forward-backward Extrusion

The extruded shapes of forward-backward extrusion in Fig. 5.19 for experimental and simulation results showed differences and the experimental values for punch load curve was fluctuated as shown in Fig. 5.20. This is mainly caused by the improper design of the die where it was designed with three segments as shown in Fig. 5.19. During metal forming process, material was flowed out from the gaps between the segments of dies and lead to material loss. The average percentage error obtained was 10%.

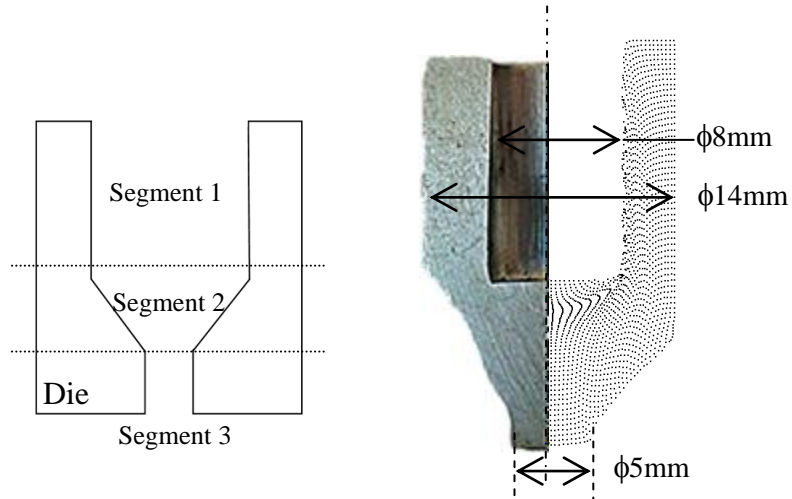


Figure 5.19: Comparison for extruded shapes between experiment and calculation in forward-backward extrusion.  
(mesh size  $M = 0.5\text{mm}$  and time step  $T = 0.05\text{s/step}$  and experimental punch rate = 2mm/min).

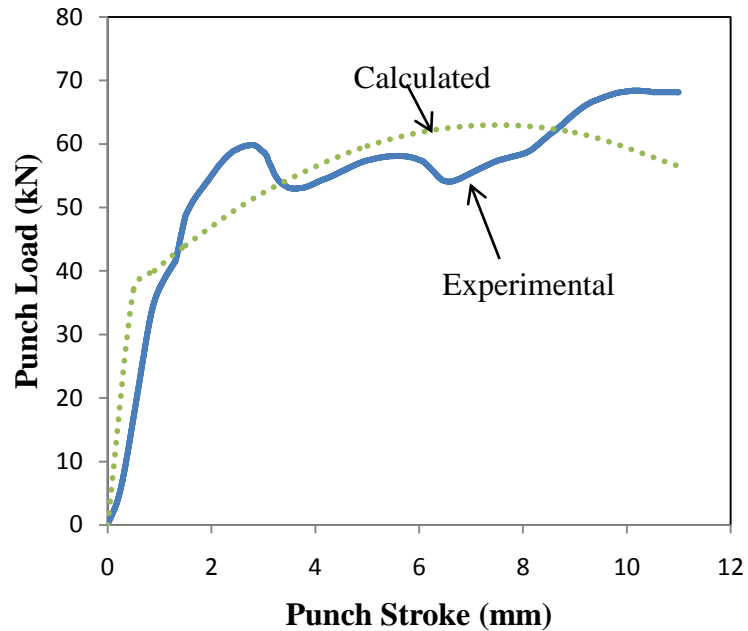


Figure 5.20: Comparison of punch load curves between experiment and calculation in forward-backward extrusion.  
(mesh size  $M = 0.5\text{mm}$  and time step  $T = 0.05\text{s}/\text{step}$ ).

Table 5.11: Comparison of punch loads between experiment and calculation in forward-backward extrusion.  
(mesh size  $M = 0.5\text{mm}$  and time step  $T = 0.05\text{s}/\text{step}$ ).

<b>Mesh Size <math>M = 0.5\text{mm}</math> &amp; Time Step <math>T = 0.05\text{s}/\text{step}</math></b>		
<b>Punch Stroke (mm)</b>	<b>Punch Load (kN)</b>	
	<b>Experimental</b>	<b>Calculated</b>
<b>3</b>	58.75	52.30
<b>5</b>	57.39	59.68
<b>7</b>	55.41	62.83
<b>9</b>	64.81	61.77
<b>11</b>	68.12	56.50
<b>Average Percentage Error (%)</b>		10

## 5.4 Double Cup Extrusion

The extruded shapes of double cup extrusion in Fig. 5.21 for experimental and simulation results were identical. Calculated and experimental punch load curves were compared in Fig 5.22. The average percentage error obtained was 5%.

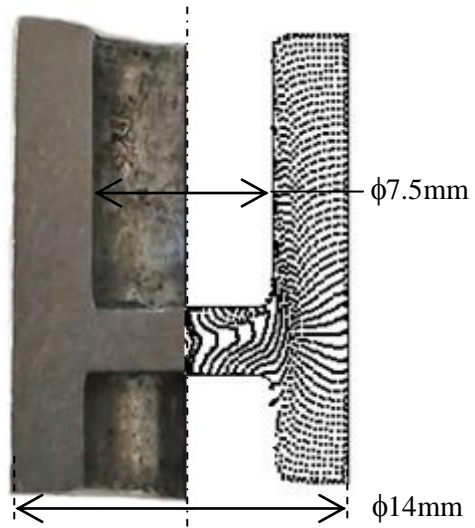


Figure 5.21: Comparison for extruded shapes between experiment and calculation in double cup extrusion.

(mesh size  $M = 0.5\text{mm}$  and time step  $T = 0.05\text{s/step}$  and experimental punch rate =  $2\text{mm/min}$ ).

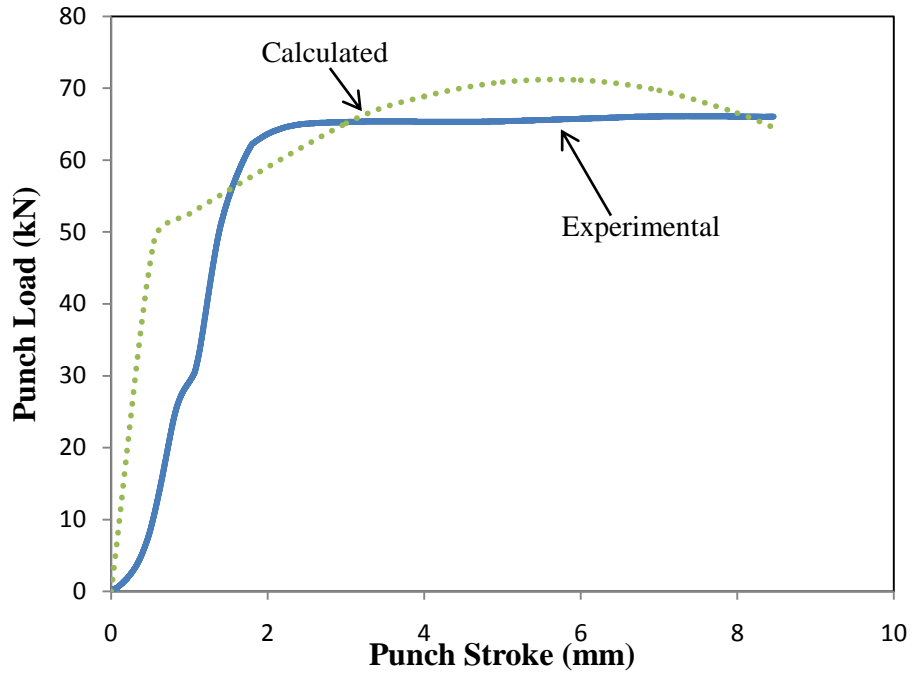


Figure 5.22: Comparison of punch load curves between experiment and calculation in double cup extrusion.  
(mesh size  $M = 0.5\text{mm}$  and time step  $T = 0.05\text{s}/\text{step}$ ).

Table 5.12: Comparison of punch loads between experiment and calculation in double cup extrusion.  
(mesh size  $M = 0.5\text{mm}$  and time step  $T = 0.05\text{s}/\text{step}$ ).

Mesh Size $M = 0.5\text{mm}$ & Time Step $T = 0.05\text{s}/\text{step}$		
Punch Stroke (mm)	Punch Load (kN)	
	Experimental	Calculated
3	65.35	65.13
4	65.41	68.85
5	65.78	70.86
6	66.10	71.15
7	66.10	69.72
Average Percentage Error (%)		5

## 5.5 Axi-symmetric Ring Cup Extrusion

The extruded shapes of axi-symmetric ring cup extrusion in Fig. 5.23 for experimental and simulation results showed slight different. Calculated and experimental punch load curves were compared in Fig 5.24. The average percentage error in Table 5.13 showed 8%.

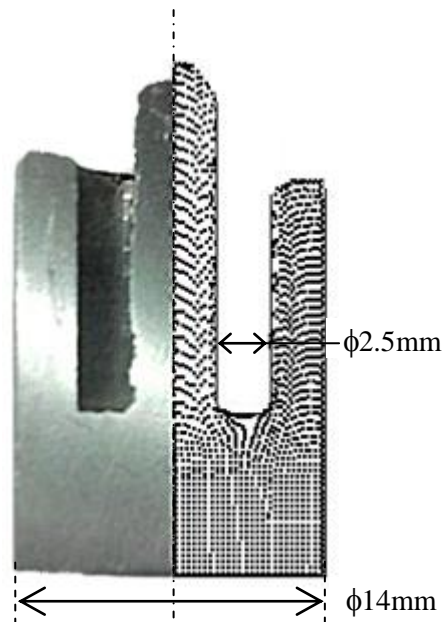


Figure 5.23: Comparison for extruded shapes between experiment and calculation in axi-symmetric ring cup extrusion.  
(mesh size  $M = 0.5\text{mm}$ , time step  $T = 0.05\text{s/step}$  and experimental punch rate = $2\text{mm/min}$ ).

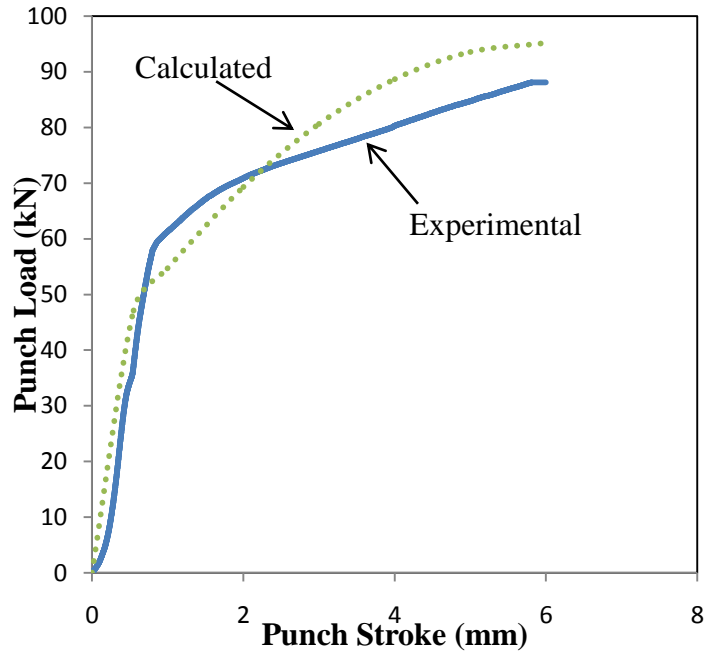


Figure 5.24: Comparison of punch load curves between experiment and calculation in axi-symmetric ring cup extrusion.  
(mesh size  $M = 0.5\text{mm}$  and time step  $T = 0.05\text{s}/\text{step}$ ).

Table 5.13: Comparison of punch loads between experiment and calculation in axi-symmetric ring cup extrusion.  
(mesh size  $M = 0.5\text{mm}$  and time step  $T = 0.05\text{s}/\text{step}$ ).

Mesh Size $M = 0.5\text{mm}$ & Time Step $T = 0.05\text{s}/\text{step}$		
Punch Stroke (mm)	Punch Load (kN)	
	Experimental	Calculated
2	70.90	59.28
3	75.79	80.61
4	80.32	88.70
5	84.75	93.57
6	88.10	95.20
Average Percentage Error (%)		8

## 5.6 Sheet Metal Clinching

The extruded shapes for experimental and simulation results in Fig. 5.25 were identical. Calculated and experimental punch load curves were compared in Fig 5.26. The average percentage error in Table 5.14 was 9%.

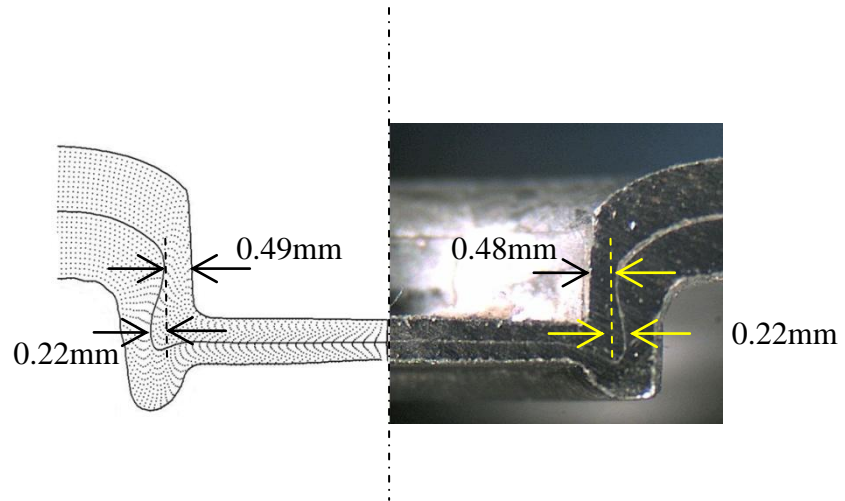


Figure 5.25: Comparison for extruded shapes between experiment and calculation in sheet metal clinching.  
(mesh size  $M = 0.5\text{mm}$  and time step  $T = 0.05\text{s}/\text{step}$ ).

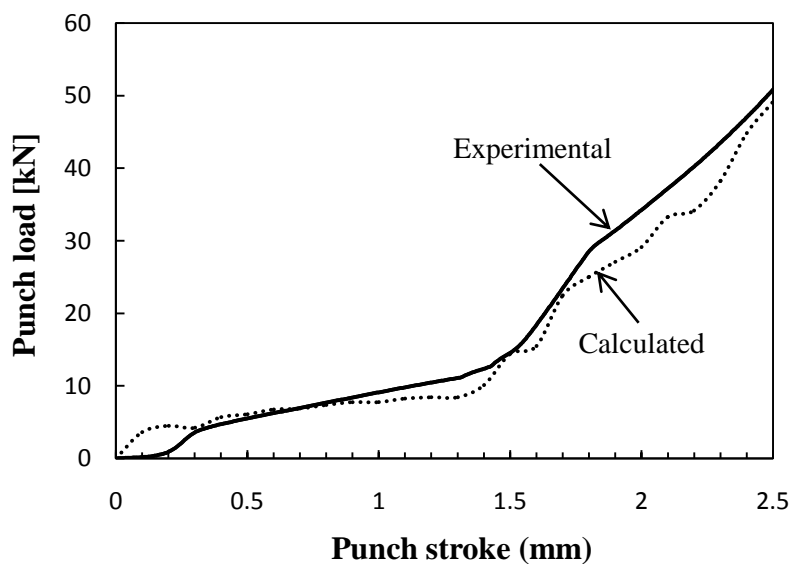


Figure 5.26: Comparison of punch load curves between experiment and calculation in sheet metal clinching.  
(mesh size  $M = 0.5\text{mm}$  and time step  $T = 0.05\text{s}/\text{step}$ ).

Table 5.14: Comparison of punch loads between experiment and calculation in sheet metal clinching  
 (mesh size  $M = 0.5\text{mm}$  and time step  $T = 0.05\text{s/step}$ ).

<b>Mesh Size <math>M = 0.5\text{mm}</math> &amp; Time Step <math>T = 0.05\text{s/step}</math></b>		
<b>Punch Stroke (mm)</b>	<b>Punch Load (kN)</b>	
	<b>Experimental</b>	<b>Calculated</b>
<b>0.5</b>	5.50	6.08
<b>1.0</b>	9.11	7.75
<b>1.5</b>	14.57	14.42
<b>2.0</b>	34.39	29.14
<b>2.5</b>	51.01	49.15
<b>Average Percentage Error (%)</b>		9

## **CHAPTER 6**

### **CONCLUSIONS AND FUTURE WORK**

#### **6.1 Conclusions**

Simulations for backward extrusion were carried out to study the sensitivity of mesh size  $M$  and time step  $T$  in Eulerian mesh. The simulation results were compared with experimental results in terms of extruded shape and punch load. With maximum number of 1600 nodal points, 1600 elements and 1600 markers, the results showed:-

1. Higher numbers of empty elements or voids were encountered in Mesh size  $M = 0.3\text{mm}$  due to limit of markers which lead to a sudden drop of punch load.
2. With mesh size  $M = 0.7\text{mm}$ , the boundary lines were coarse compared to lower mesh size and caused higher percentage errors.
3. Markers in time step  $T = 0.5\text{s}/\text{step}$  were scattered in the inner surface of workpiece and affected the quality of extruded shapes.
4. Slower time step  $T = 0.005\text{s}/\text{step}$  contributed to the highest computational time but did not improve the accuracy of punch loads obtained significantly especially with mesh size  $M = 0.7\text{mm}$ .
5. The most appropriate simulation parameters under the mentioned numbers of nodal points, elements and markers were mesh size  $M = 0.5\text{mm}$  and time step  $T = 0.05\text{s}/\text{step}$ .

Simulation parameter of mesh size  $M = 0.5\text{mm}$  and time step  $T = 0.05\text{s}/\text{step}$  were applied to others metal forming such as forward-backward, double cup, axi-symmetric ring cup extrusion and sheet metal clinching. The results from experiments and calculations were compared in term of extruded shape and punch loads. The percentage errors were ranging from 3 to 10%. The extruded shapes and punch load curves were well predicted using Eulerian scheme except the forward-backward extrusion due to the inappropriate die design.

## 6.2 Contributions

This study had contributed to the understanding of the behaviours for Eulerian mesh and sensitivities for mesh size and time step in FEM simulation on metal forming such as forging and sheet metal clinching. Besides, the effectiveness of Eulerian mesh was tested on backward extrusion, forward-backward extrusion, double cup extrusion, axi-symmetric ring cup extrusion and compared with experimental results. The extruded shapes for the forging and sheet metal clinching processes provide the information of flow patterns during deformation. In addition, investigation on punch load curves contributed to the understanding of the load distribution and deformation behaviour of the forging and sheet metal clinching processes.

### **6.3 Future Work**

There are possibilities and improvements to be done to expand this research in future:-

1. The study can be expanded to the sensitivity of number of markers and markers distance.
2. Application of Eulerian scheme can be expanded to hot forging processes.
3. As the rapid advancement of computers technologies, the present two-dimensional simulation model can be improved to three-dimensional approach.

## REFERENCES

- Alfaro, I., Yvonnet, J., Chinesta, F., Cueto, E., 2007. A study on the performance of natural neighbor-based Galerkin methods. *International Journal for Numerical Methods in Engineering*, 7(12), pp. 1436-1456.
- Altan, T., Ngaile, G. and Shirgaokar, M., 2003. State of cold forging technology in global competition. *Proceedings of the International Conference on New Developments Bulk Forging*, The Ohio State University.
- Behzad, S., Kjell, M. and Alf, S., 1994. Implicit and dynamic explicit solutions of blade forging using the finite element method. *J. Mater. Process. Technol.*, 45 , pp. 69-74.
- Boman, R., Papeleux, L., Bui, Q.V. and Ponthot, J.P., 2006. Application of the Arbitrary Lagrangian Eulerian formulation to the numerical simulation of cold roll forming process. *Journal of Materials Processing Technology*, 177, pp. 621-625.
- Edwin, H., Chang, K., Tulian, G., Yoon, S., Michimaro, K. and Chen, J., 1999. A Structural Nonlinear Analysis Workspace (SNAW) based on meshless methods. *Advances in Engineering Software*, 30, pp. 153-175.

Filice, L., Alfaro, I., Gagliardi, F., Cueto, E., Micari, F. and Chinesta, F., 2009. A preliminary comparison between finite element and meshless simulations of extrusion. *Journal of Materials Processing Technology*, 209, pp. 3039-3049.

Gadala, M.S., Movahhedy, M.R. and Wang, J., 2002. On the mesh motion for ALE modeling of metal forming processes. *Finite Elements in Analysis and Design*, 38, pp. 435-459.

Khaleed, H.M.T., Samad, Z., Othman, A.r., Phili, S.C., Slaman, A.N.J., Irfan, A.B., Hakim, S.S., Quadir, G.A. and Abdullah A.B., 2009. A study on cold forging die design using different techniques. *Modern Applied Science*, 3 (3), pp. 143-154.

Makinouchi, A., 1991. Contact descriptions in finite element simulation of metal forming processes. *Computer Aided Innovation of New Materials*, pp. 597-602.

Mori, K., Osakada, K. and Fukuda, M., 1983. Simulation of severe plastic deformation by finite element method with spatially fixed elements. *Int. J. Mech. Sci.*, 25 (11), pp. 775-783.

Mori, K., Wang, C.C. and Osakada, K., 1996. Inclusion of elastic deformation in rigid-plastic finite element analysis. *Int. J. Mech. Sci.*, 38 (6), pp. 621-631.

Oh, S.I., Lahoti, G.D. and Altan, T., 1982. Application of a rigid-plastic finite-element method to some metalforming operations. *Journal of Mechanical Working Technology*, 6, pp. 277-290.

Osakada, K., Nakano, J. and Mori, K., 1982. Finite element method for rigid-plastic analysis of metal forming-formulation for finite deformation. *Int. J. Mech. Sci.*, 24 (8), pp. 459-468.

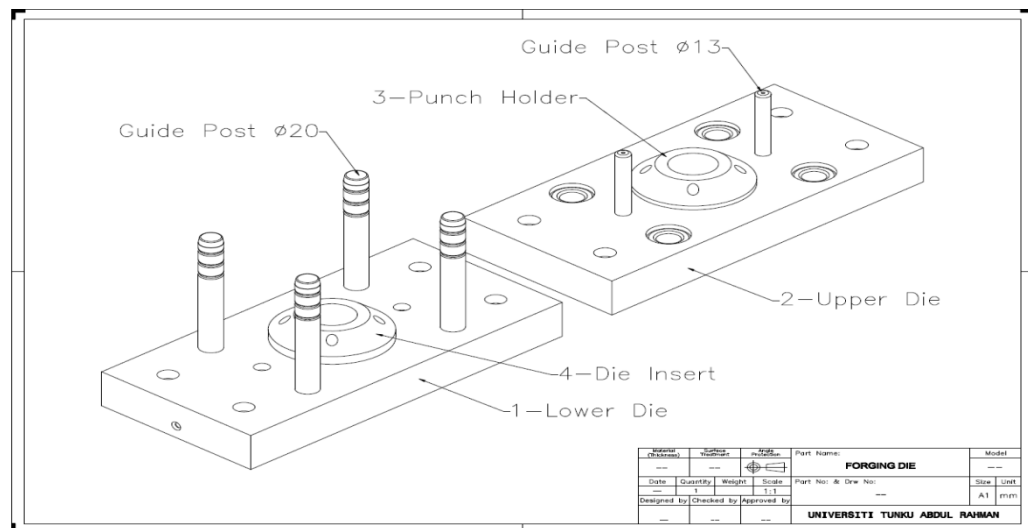
Williams, A.J., Corft, M. and Cross, M., 2002. Computational modeling of metal extrusion and forging processes. *Journal of Material Processing Technology*, 152-156, pp. 573-582.

Williams, A.J., Slone, A.K., Croft, T.N. and Cross, M., 2010. A mixed Eulerian-Lagrangian method for modelling metal extrusion processes. *Computer Methods in Applied Mechanics and Engineering*, 199, pp. 2123-2134.

Yoon, S. and Chen, J.S., 2002. Accelerated meshfree method for metal forming simulation. *Finite Elements in Analysis and Design*, 38, pp. 937-948.

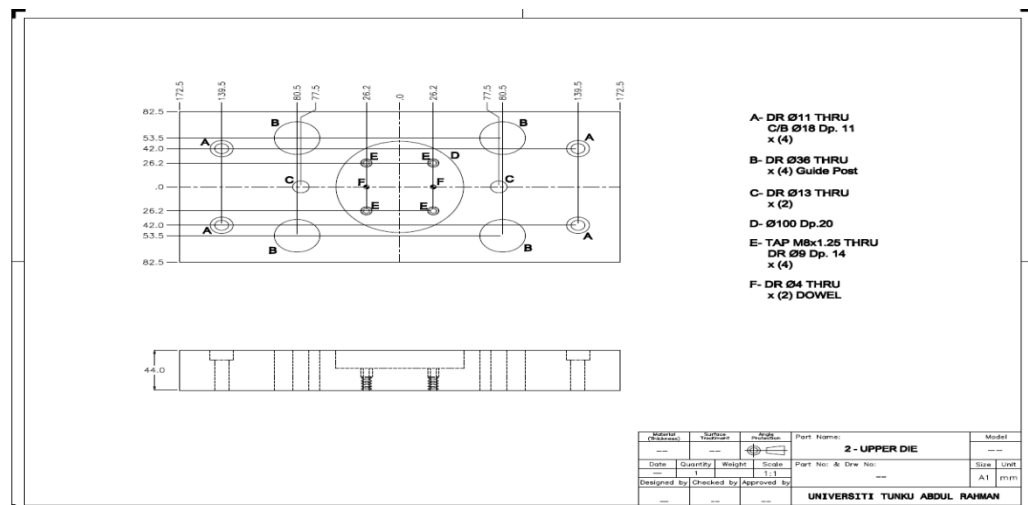
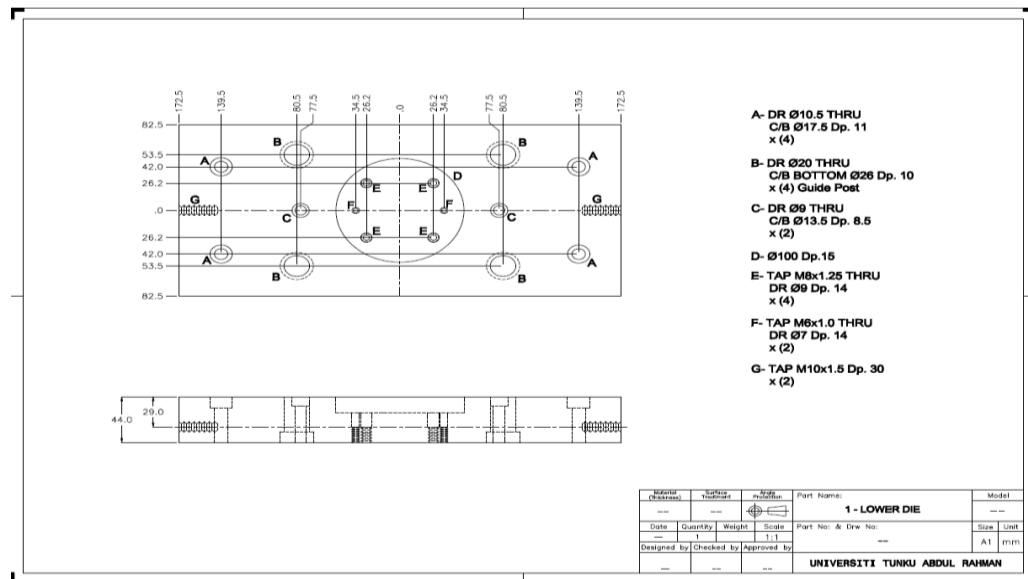
## APPENDIX A

### DIE SET



## APPENDIX B

### BOTTOM AND UPPER DIE



## APPENDIX C

### INSERT HOLDER

